JOURNAL OF GEOPHYSICAL RESEARCH, VOL. 114, D02207, doi:10.1029/2007JD009587, 2009

Impact of biomass burning aerosols on precipitation in the Amazon: A modeling case study

J. A. Martins,[1,2] M. A. F. Silva Dias,[2,3] and F. L. T. Gonçalves[2]

Received 10 November 2007; revised 20 October 2008; accepted 20 November 2008; published 29 January 2009.

[1] A study of the potential role of aerosols in modifying clouds and precipitation is presented using a numerical atmospheric model. Measurements of cloud condensation nuclei (CCN) and cloud size distribution properties taken in the southwestern Amazon region during the transition from dry to wet seasons were used as guidelines to define the microphysical parameters for the simulations. Numerical simulations were carried out using the Brazilian Development on Regional Atmospheric Modeling System, and the results presented considerable sensitivity to changes in these parameters. High CCN concentrations, typical of polluted days, were found to result in increases or decreases in total precipitation, depending on the level of pollution used as a reference, showing a complexity that parallels the aerosol-precipitation interaction. Our results show that on the grids evaluated, higher CCN concentrations reduced low-to-moderate rainfall rates and increased high rainfall rates. The principal consequence of the increased pollution was a change from a warm to a cold rain process, which affected the maximum and overall mean accumulated precipitation. Under polluted conditions, cloud cover diminished, allowing greater amounts of solar radiation to reach the surface. Aerosol absorption of radiation in the lower layers of the atmosphere delayed convective evolution but produced higher maximum rainfall rates due to increased instability. In addition, the intensity of the surface sensible heat flux, as well as that of the latent heat flux, was reduced by the lower temperature difference between surface and air, producing greater energy stores at the surface.

Citation: Martins, J. A., M. A. F. Silva Dias, and F. L. T. Gonçalves (2009), Impact of biomass burning aerosols on precipitation in the Amazon: A modeling case study, *J. Geophys. Res.*, *114*, D02207, doi:10.1029/2007JD009587.

1. Introduction

[2] Atmospheric aerosols can affect climate in a number of ways. *Jacobson* [2002] identified 12 possible effects of aerosols on climate. For most of those effects, little or no knowledge has been accumulated and there are many uncertainties associated with their measurements or assimilation in current models [*Stier et al.*, 2007]. However, airborne measurements over human-influenced areas have shown that aerosols impact directly on cloud properties in different ways [*Ackerman et al.*, 2000]. First, such aerosols can have a direct impact on the energy balance by diffusing and reflecting solar radiation back into space (direct effect). This occurs primarily as a result of natural processes and human activities, such as industry, fossil fuel and biomass burning. Aerosols also serve as cloud condensation nuclei (CCN), modifying the microphysics, radiative properties and cloud lifetime (indirect effect). The indirect effects of aerosols are typically categorized as one of two types. The first type involves an increase in aerosol concentrations, which increases droplet concentration and decreases droplet size for fixed liquid water content [*Twomey*, 1974]. The second one involves a reduction in cloud droplet size, which affects precipitation efficiency, tending to increase the liquid water content and cloud lifetime [*Albrecht*, 1989]. Both types of indirect effects cool the Earth by reflecting solar radiation back into space. However, studies involving absorbing aerosols suggest that anthropogenic aerosols cause less cooling than has commonly been assumed [*Hansen et al.*, 1997; *Schuster et al.*, 2005; *Ramanathan and Carmichael*, 2008]. In addition, detailed investigations performed using numerical models suggest a substantial effect of aerosols not only on the dynamics of single clouds, but also on the dynamics of atmospheric motions from convective [*Khain et al.*, 2005] to, possibly, global scales [*Lohmann and Feichter*, 2005].

[3] Most recent studies focus on the global aspect of the anthropogenic aerosol effects, comparing polluted and non-polluted areas or the land-ocean contrast. Some of these studies have evaluated the aerosol-cloud system using satellite images as described by *Platnick et al.* [2003], neglecting questions related to precipitation development [*Kaufman and Nakajima*, 1993; *Kaufman and Fraser*, 1997; *Rosenfeld*, 1999; *Breon and Doutriaux-Boucher*, 2005; *Kawamoto and*

[1]Department of Environmental Engineering, Federal University of Technology-Paraná, Londrina, Brazil.
[2]Department of Atmospheric Science, University of São Paulo, São Paulo, Brazil.
[3]Centro de Previsão de Tempo e Estudos Climáticos, Cachoeira Paulista, Brazil.

0148-0227/09/2007JD009587$09.00

Nakajima, 2003; *Kawamoto*, 2006]. Another significant part of these studies is performed by using global models [*Boucher and Lohmann*, 1995; *Nober et al.*, 2003; *Suzuki et al.*, 2004; *Penner et al.*, 2006; *Anderson et al.*, 2003; *Lohmann and Feichter*, 2005; *Lohmann et al.*, 2007]. In the global focus, as in the mentioned studies, the precipitation process is primarily characterized according to its macroscopic properties, such as cloud cover, cloud optical depth, cloud albedo and effective particle radius. Only a small number of studies have focused on precipitation development. To date, *Rosenfeld et al.* [2006] discuss the possible mechanisms for the maintenance of the precipitation structure, emphasizing the microphysical effects caused by aerosols, not revealed by satellite inferences.

[4] Part of those investigations involving precipitation process as a whole are conducted using numerical models. The effect of aerosols on cloud microphysics and dynamics is studied by *Khain et al.* [2005], using a spectral microphysics two-dimensional cloud model. In the simulated maritime scenario, aerosols promoted a rapid formation of raindrops that fell down through cloud updrafts. Clouds developing in a continental-type scenario, which is characterized by an increase in the concentration of small cloud condensation nuclei, provoked the formation of a large number of small droplets with a low collision rate. This resulted in a time delay of raindrop formation, slowing the downdrafts caused by the falling raindrops. The latent heat release was also increased by condensation and freezing of water that rises to the freezing level, which promoted larger updrafts.

[5] *Lin et al.* [2006] presented a particularly interesting example of the empirical relationships between aerosol- and precipitation-related parameters, based on satellite data from the Moderate Resolution Imaging Spectroradiometer and Tropical Rainfall Measuring Mission instruments. The authors showed that, during the transition from the dry to wet season in two different years, an increase in aerosol concentration was associated with a change in the probability density function of rainfall rates, increasing the number of events presenting higher rainfall rates, as well as increasing the water paths (liquid and ice), increasing high-level cloud cover and decreasing cloud top temperatures. The present study attempts to explain these empirical relationships.

[6] The primary goal of this study was to investigate the effects of aerosols on the evolution of microphysical processes in the convective clouds that typically develop near the end of the dry season in the Amazon region. This was achieved using numerical modeling under various CCN concentration and cloud spectra parameter scenarios. In addition, aerosol-radiation interactions were evaluated in a specific scenario. The aerosol-cloud interaction theme has been extensively discussed, and there are empirical and numerical data showing the aerosol effects on clouds and precipitation onset. However, the effects that aerosols have on the surface accumulation of precipitation have received less attention. In this study, we discuss those effects, especially in relation to convective clouds, which produce considerable quantities of precipitation over the Amazon region. This is the predominant structure of precipitation occurring in the Amazon region, and there are observational data indicating that precipitation is sensitive to CCN concentrations [*Silva Dias et al.*, 2002a; *Williams et al.*, 2002].

[7] In this investigation, we used a high-resolution configuration of the Brazilian Development on Regional Atmospheric Modeling System (BRAMS). Data obtained during the Large-Scale Biosphere-Atmosphere Experiment in Amazonia (LBA) were used as references. In recent years, a variety of LBA results have been published. Available data range from those related to the mesoscale effects of tropical deforestation [*Dolman et al.*, 1999] to those describing biosphere-atmosphere interactions, interactions among cloud and rain processes [*Silva Dias et al.*, 2002a], aerosol-cloud interactions [*Andreae et al.*, 2004] and the transport of biomass burning emissions [*Freitas et al.*, 2006]. Specific data used in the numerical simulations were CCN concentrations and shape parameters of gamma functions representing cloud droplet spectra, as described by *Martins et al.* [2004] and *Gonçalves et al.* [2008]. The data sets were compiled from aircraft flyover measurements, taken in the southwestern Amazon region between September and October of 2002, and are the same as those used in a previous study [*Andreae et al.*, 2004]. The implications of higher aerosol concentrations for the development of convective mixed-phase clouds are discussed. The impact that higher aerosol concentrations have on total accumulated precipitation, microphysical/dynamic properties of clouds and the net radiative balance at the surface, are also evaluated.

2. Model and Data

2.1. BRAMS Overview

[8] The RAMS mesoscale model is a nonhydrostatic terrain-following sigma-coordinate model designed to simulate mesoscale and regional-scale atmospheric circulation. It was initially developed at Colorado State University but later evolved to a community mesoscale model and is continuously being improved by contributions from users at various institutions worldwide.

[9] The RAMS model utilizes the full set of nonhydrostatic, Reynolds-averaged primitive equations [*Tripoli and Cotton*, 1982]. The model solution is advanced in time by using a hybrid time stepping scheme in which the momentum and scalar fields are integrated using a second-order accurate leapfrog scheme and a forward scheme, respectively. The RAMS uses a terrain-following coordinate designated sigma-z in the vertical scheme, and numerous options are available for the boundary conditions, turbulence parameterization, radiation schemes, microphysical parameterizations and surface schemes. The present study addresses only cloud microphysical parameterization. For a more general discussion of the numerous options available in the model, readers are referred to *Pielke et al.* [1992] and *Cotton et al.* [2003]. The Brazilian version of the model (BRAMS) is the result of changes incorporated by Brazilian users in recent years, which include a simple photochemical module [*Freitas et al.*, 2005], a plume rise mechanism [*Freitas et al.*, 2006] and a soil moisture scheme [*Gevaerd et al.*, 2006]. Validation of the BRAMS for use in Amazon region simulations was presented by *Freitas et al.* [2007].

2.1.1. BRAMS Configurations

[10] Atmospheric fields (Brazilian Center for Weather Prediction and Climate Studies General Circulation Model, 200 km) and soil humidity [*Gevaerd et al.*, 2006] were used

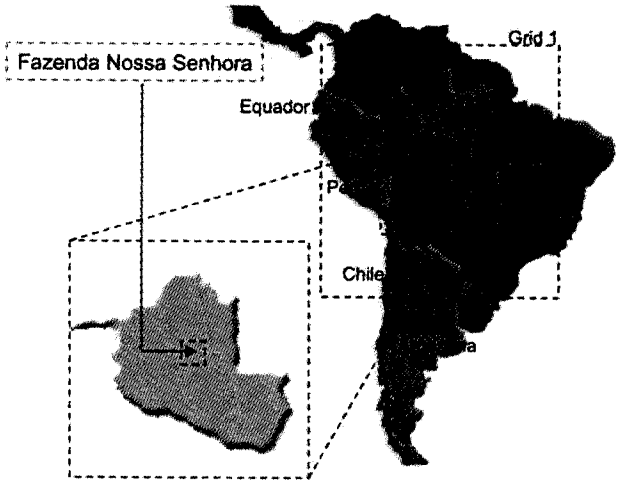

Figure 1. Interactive nested grids 1, 2, and 3, centered on the Brazilian State of Rondônia (inset) and specifically on the pasture site of grid 4 (Fazenda Nossa Senhora).

as initial and boundary conditions. The grid specifications used during the numerical simulations run in the present study are described in Table 1. Figure 1 shows four interactive nested grids, centered on the Fazenda Nossa Senhora (FNS) pasture site in the southwestern Amazon region (10.92°S; 62.41°W), which was chosen in order to represent a region in which there is considerable deforestation-related biomass burning. Other data sets were also used: topography (United States Geological Survey, 1-km resolution); sea surface temperature (National Center for Environmental Prediction, weekly readings); soil features (United States Geological Survey, 1-km resolution); physical parameterizations of radiation [*Chen and Cotton*, 1983]; radiative lateral boundary conditions [*Klemp and Wilhelmson*, 1978]; surface (Land Ecosystem-Atmosphere Feedback 2 [*Walko et al.*, 2000]); turbulence [*Mellor and Yamada*, 1974, 1982]; and convection (for grids 1 and 2 [*Grell*, 1993]). The two-moment cloud model [*Meyers et al.*, 1997] was applied to microphysical parameterization and is discussed in the following section.

2.1.2. Cloud Microphysics

[11] The BRAMS bulk microphysical parameterization predicts mixing ratios and number concentrations for rain, pristine ice, snow, aggregates, graupel, hail and cloud water. The microphysics option used in the present study involved the activation of all water types. Physical processes represented in the model include vapor/heat diffusion, collision/coalescence (between all possible hydrometeor type pairs, including self-collection), melting, freezing, heterogeneous nucleation of ice through contact/deposition freezing, homogeneous nucleation of cloud droplets/haze into ice crystals, secondary production of ice and shedding of liquid water by hail, as well as collisional breakup and sedimentation. During the simulations, ice crystal behavior, which varies depending on cloud temperature and humidity, was classified as producing one of five ice crystal types: columns, needles, hexagonal plates, dendrites or rosettes. The most recent two-moment cloud model [*Meyers et al.*, 1997] employs a direct, noniterative implicit algorithm for equations simultaneously representing vapor and heat diffusion between the air and among all hydrometeor species. The implicit solution to the system of diffusion equations also provides a stable, accurate solution to hydrometeor temperatures, vapor temperatures and mixing ratios. From these, an accurate supersaturation value can be derived, assuming that there is no concurrent CCN activation.

[12] The CCN activation mechanism included in the BRAMS model employs a precomputed table of CCN concentration and droplet sizes based on integrations of a detailed cloud model. The table is based on five atmospheric parameters: temperature; two CCN activation parameters (the well-known empirical parameters C and k in the power law parameterization [*Twomey and Wojciechowski*, 1969]); the dynamic supersaturation production rate (the rate at which supersaturation increases as a result of vertical advection); and the fraction of CCN already activated. During the simulations, the precomputed values are accessed to determine the number of newly activated cloud droplets during each time step. The cloud droplets are nucleated from a combination of the precomputed table values, the CCN concentration determined in the previous time step and the supersaturation production rate. The CCN field is initialized by default from the concentration specified by the user but evolves in time thereafter. Although there is no scavenging removal or CCN source involved, there is advective and diffusive transport. The CCN concentration is given as units per kilogram of air, which is roughly equal to number per cubic meter in the lower troposphere, although it is less than that at higher levels.

[13] A general description of the precipitation formation parameterization used in the BRAMS is given by *Flatau et al.* [1989], *Pielke et al.* [1992], *Walko et al.* [1995] and *Meyers et al.* [1997]. Descriptions concerning the specific processes parameterizations can be found in a number of other studies. A variety of physical mechanisms promoting nucleation of pristine ice crystals is parameterized in the model. Deposition nucleation and condensation freezing are represented by a single empirically based parameterization described by *Meyers et al.* [1992]. Parameterizations of the number of crystals produced by contact nucleation are described by *Cotton et al.* [1986] and *Meyers et al.* [1992]. Parameterization of the homogeneous nucleation of supercooled water is derived from empirical data following *DeMott et al.* [1994].

Table 1. Grid Specifications for the Numerical Simulations[a]

	Grid 1	Grid 2	Grid 3	Grid 4
Number of grid points (x, y, z)	(62, 62, 43)	(62, 62, 43)	(122, 122, 43)	(42, 42, 43)
Horizontal grid points (x, y)	(62, 62, 43)	(62, 62, 43)	(4 km, 4 km)	(1 km, 1 km)
Time step (s)	120	30	7.5	1.875

[a]Start time to end time is 0000 UTC, 23 September 2002 to 0000 UTC, 24 September 2002. Vertical grid spacing is 43 levels with variable stretching factor. Grid center is 10.92°S; 62.41°W (site is Fazenda Nossa Senhora).

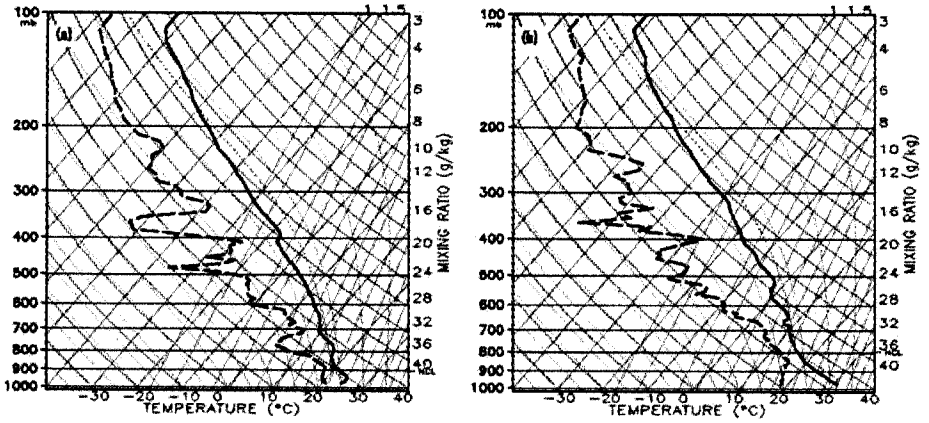

Figure 2. Fazenda Nossa Senhora sounding data at (a) 0800 and (b) 1200 LT on 23 September 2002.

The secondary production of ice crystals follows the Hallett-Mossop ice multiplication theory [*Hallett and Mossop*, 1974; *Mossop*, 1976], with additional modifications proposed by *Cotton et al.* [1986]. The transition from cloud droplets to raindrops due to collision and coalescence of cloud droplets (auto conversion) is described by *Berry and Reinhardt* [1974a, 1974b]. The stochastic collection equation is solved in three-dimensional precomputed tables in order to predict mixing ratio [*Verlinde et al.*, 1990] and number concentration [*Meyers et al.*, 1997]. *Verlinde and Cotton* [1993] parameterized the breakup coalescence efficiency into the self-collection equation. The new developments in the RAMS physics since first versions are described by *Walko et al.* [2000] and *Cotton et al.* [2003]. Many microphysical processes parameterized in RAMS is also discussed by *Khain et al.* [2000] in a review of the state-of-the-art numerical modeling of cloud microphysics.

2.2. Observed Data

2.2.1. Atmospheric Conditions

[14] The day 23 September 2002 was selected because it adequately represents the typical atmospheric conditions prevailing during the transition from the dry season to the wet season. The thermodynamic conditions predominant in the simulation day are shown in Figure 2. This transition period is characterized by the occurrence of local and isolated precipitation events, which are occasionally quite intense [*Williams et al.*, 2002]. In addition, the data set for the selected day was quite complete (cloud and CCN properties obtained during aircraft flyovers; aerosol data; sounding data; satellite images; surface automated weather station data; and data from the monitoring of hot spots associated with biomass burning). The temporal evolution of hot spots in the grid 3 domain on the selected day is shown in Figure 3.

[15] The 23 September case presented characteristics similar to those seen on previous days and typical of the end of the dry season in the southwestern Amazon region. *Vestin et al.* [2007] evaluated CCN data obtained at the FNS pasture location, which is also in the southwestern Amazon, and noted heavy smoke during the 21–23 September period. It is likely that the convection triggering mechanism was associated with local radiative heating as well as with topographic forcing, which is quite common in this region [*Silva Dias et al.*, 2002b]. In general, convection began in late morning, with bands of shallow clouds developing in the Rondônia area (Figure 4a). These shallow cumuli formed near noon and rapidly evolved to a few deep cells observed in midafternoon (Figures 4b and 4c). The development of such cells was common within the 150-km radar range in the midafternoon. A very clear example of a deep convective cell formed on 23 September can also be seen in the satellite image (Figure 4d) and is discussed further below. Although rain was not recorded at the FNS site (since the cell developed in the vicinity), that particular convective cell developed into a strong thunderstorm, featuring high winds and lightning, in the early evening. The occurrence of such isolated events near the FNS site might explain the slight decrease observed in CCN concentrations during the days following 23 September.

[16] On 23 September, the boundary layer presented behavior typical of the dry season, with full vertical development (1600 m in depth). At approximately 1400 LT, the potential temperature and specific humidity recorded at the FNS site were 306.5°K and 13.5 g/kg, respectively (averaged over the boundary layer depth). Low-to-moderate wind speeds were observed within and above the boundary layer

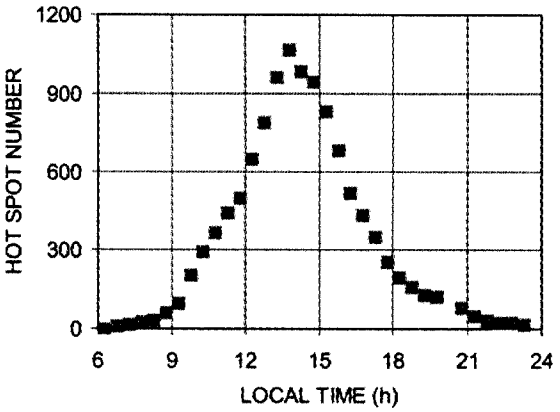

Figure 3. Hot spot number evolution in an equivalent area to grid 3 (240,000 km^2) on 23 September 2002. Data provided by Elaine M. Prins (National Oceanic and Atmospheric Administration/National Environment Satellite Data and Information Service).

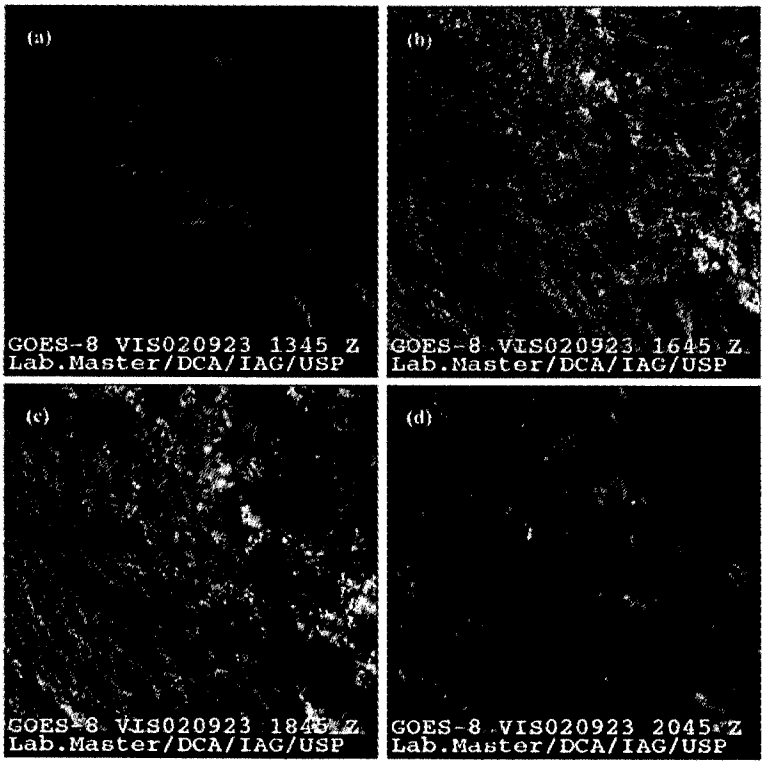

Figure 4. Visible images from the Geostationary Operational Environmental Satellite (GOES) showing the daily evolution of cloud cover on 23 September 2002.

(2 m/s from the south and 4–8 m/s from the north, respectively). The change in wind speed and direction with altitude, together with the convective transport of humidity by shallow clouds (Figure 4), might be responsible for the opposite trend in the humidity vertical profile (Figure 5).

2.2.2. CCN and Cloud Droplet Spectra

[17] Field measurements of CCN and cloud size distributions taken during the LBA campaign revealed distinct differences between the characteristics of clean atmospheric conditions and those of polluted atmospheric conditions. The measurements were made over the southwestern Amazon region during September and October of 2002, thereby focusing on the transition from dry to wet seasons. During that period, analysis of CCN concentrations in the boundary layer revealed an general trend toward a decrease, mean values falling from above 1200 cm^{-3} to below 300 cm^{-3} (for supersaturation of 0.5%). The comparison between clean and polluted areas revealed differences of the same order in terms of CCN concentrations. Complete descriptions of the CCN properties observed in the boundary layer and at the surface is given by *Martins et al.* [2004] and *Vestin et al.* [2007], respectively.

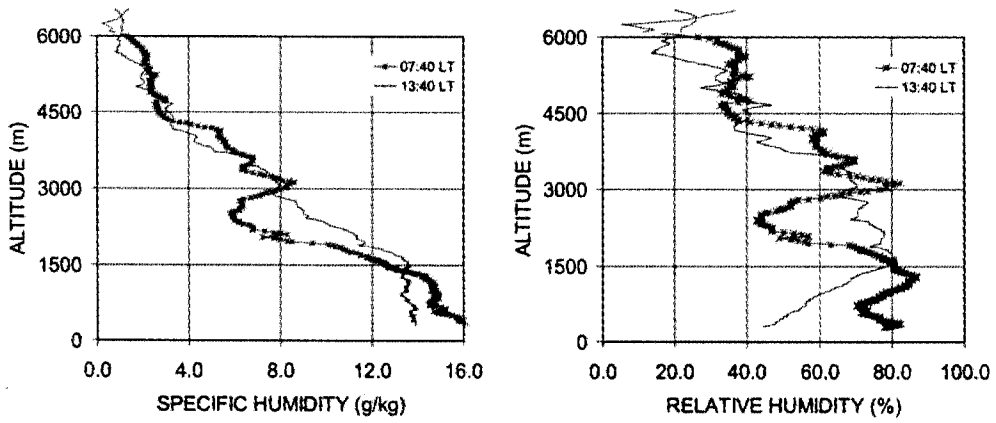

Figure 5. Vertical profile of (left) specific humidity and (right) relative humidity at two different time points on 23 September 2002.

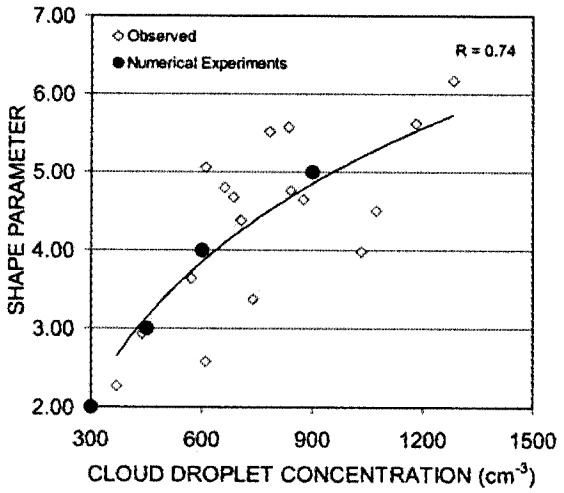

Figure 6. Observed shape parameters versus observed cloud droplet concentrations, together with the corresponding values adopted in the numerical simulations (solid circles).

[18] Cloud droplet size distributions in regions with extremely different aerosol concentrations were also analyzed. A gamma distribution was used to fit the measured cloud droplet spectra, and the shape parameter was used as a criterion to define the best choice of spectra representation. In the BRAMS model, gamma distribution is the function used to parameterize the hydrometeor types. The shape of each hydrometeor type in the model can be controlled using the shape parameter of the gamma distribution. According to the values presented by *Gonçalves et al.* [2008], narrow gamma distributions optimally fit polluted conditions (shape parameter of approximately 5), whereas broad distributions are the best fits for unpolluted conditions (shape parameter of approximately 2). In conjunction with CCN concentration, the shape parameter was used in the numerical simulations conducted in the present study. Figure 6 shows the various combinations of cloud droplet concentrations and shape parameters observed with the instrumented aircraft during the field campaign.

3. Methodology

[19] The following is an overview of how the simulations were designed and organized. Five simulations were run for 23 September 2002. The first simulation involved running the model with a low CCN concentration (300 cm^{-3}) in order to represent clean atmospheric conditions that were in accordance with the observed values listed in section 2.2.2. The shape parameter for the distribution of cloud droplets and pristine ice was 2, whereas the distribution of the other hydrometeor types was specified with a shape parameter of 1. The additional parameters followed a common set of specifications as described in section 2.1.1. This numerical simulation is hereafter referred to as scenario CCN300. In the second numerical simulation, designated scenario CCN450, the CCN concentration was set at 450 cm^{-3}, the shape parameter for cloud droplets/pristine ice was 3, and the remaining parameters were the same as those used in scenario CCN300. The third and fourth simulations (scenarios CCN600 and CCN900, respectively) involved the configuration established for scenario CCN450 but with the CCN concentrations set at 600 cm^{-3} and 900 cm^{-3}, respectively, and shape parameters of 4 and 5, respectively. Figure 6 shows the shape parameters and droplet concentrations used in the numerical simulations. The fifth numerical simulation, designated scenario CCN900R, was identical to scenario CCN900, except for the fact that radiative forcing was added, as discussed in the next paragraph. The complete microphysical configuration of the numerical simulations is summarized in Table 2. In accordance with the findings of *Gonçalves et al.* [2008] and consistent (at least for CCN concentration) with observations made by *Andreae et al.* [2004], the shape parameter for cloud water and pristine ice was assumed to change from 2 under clean conditions to 5 under polluted conditions. For all other hydrometeor types, it was maintained at 1.

[20] Cloud droplet concentrations showed by *Andreae et al.* [2004] are obviously too high, at least in the clean conditions, as pointed by the authors. The trend is opposite the CCN concentration data from the static thermal-gradient diffusion chamber, since this instrument is not indicated to concentration of particles higher than 1000 cm^{-3}. In the decision to start simulation based in CCN concentration it was used the work of *Roberts et al.* [2001], who found CCN concentrations for rainy season very close to that found in clean conditions of the LBA-SMOCC campaign. Their results correspond to the first measurements of CCN in the Amazon Basin and showed values more typical of near marine locations (182 and 267 cm^{-3}, respectively at supersaturations of 0.6 and 1.0%). Concerning to the present data, it was found CCN concentrations of about 300 cm^{-3} characterizing the 8 and 9 October clean days, and even lower values for 5 October (204 cm^{-3} at 0.5% of supersaturation). In this case the measurements were performed in the clean air at the western part of the Amazon, defined by *Andreae et al.* [2004] as green ocean in their conceptual model about precipitation regimes.

Table 2. Microphysical Parameters Used in the Numerical Simulations[a]

	CCN300	CCN450	CCN600	CCN900	CCN900R
CCN concentration	300	450	600	900	900
Shape parameter for cloud droplets and pristine ice	2	3	4	5	5
Shape parameter for all remaining water types	1	1	1	1	1
Radiative effect	None	None	None	None	Absorption and reflection

[a]CCN, cloud condensation nuclei; CCN300, scenario representing "clean" conditions (CCN concentration, 300 cm^{-3}); CCN450, scenario representing "relatively clean" conditions (CCN concentration, 450 cm^{-3}); CCN600, scenario representing "moderately polluted" conditions (CCN concentration, 600 cm^{-3}); CCN900, scenario representing "polluted" conditions (CCN concentration, 900 cm^{-3}); CCN900R, scenario also representing "polluted" conditions (CCN concentration, 900 cm^{-3}) but with radiative forcing.

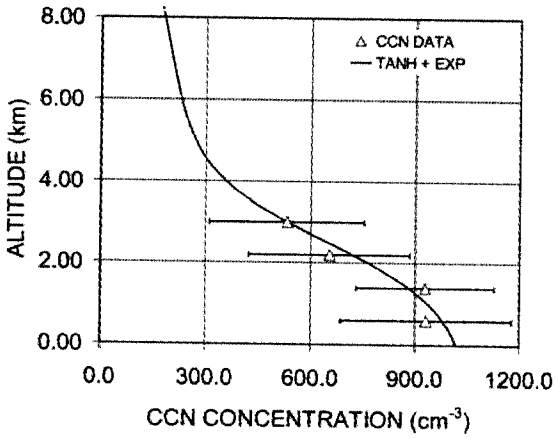

Figure 7. Vertical profile of observed cloud condensation nuclei (CCN) concentrations (triangles) and fitted curve by which radiative forcing was adjusted (solid line), both for 23 September 2003. The horizontal bars correspond to 1 standard deviation. The fitting curve is based on a combination of hyperbolic tangent (TANH) and exponential (EXP) functions.

[21] A second aspect that turn the used CCN measurements reliable is the low concentration found in the beginning of the first flight of the LBA campaign, performed very close to the Atlantic Ocean (influenced by easterly maritime air masses associated with the trade winds). For example, average CCN concentration at 0.5% supersaturation was 131 cm^{-3}. It is important to note that although biomass burning emission was present in most of the flights, the average CCN concentrations previously analyzed and used in this work do not include the measurements performed within the smoke plumes. These measurements are normally associated to pyroclouds (clouds that develop above the smoke and heat from fires). The strong difference between the pyroclouds and background measurements could disturb the data, since a significant time is necessary to perform a complete cycle of measurements in CCN concentrations. Sometimes a CCN concentration inside a pyrocloud can reach 20–30 times the background values. Therefore, the analysis included only CCN concentrations in clean and polluted background atmospheric conditions prevailing in that region while *Andreae et al.* [2004] used just smoky-cb data as indicated by their Table 1. Additionally, the ratio smoky-cb/green-ocean (see the cited work for details) is expected to be much more coherent for CCN (~2500/340) than for cloud droplets (2200/1000). The coherence (incoherence) also increases when pyro-cb data is analyzed for CCN (cloud droplets).

[22] The radiative forcing in scenario CCN900R was assumed to reduce the incoming, reflecting and absorbing solar radiation. The two effects together caused a reduction of approximately 20% in the amount of solar radiation reaching the top of troposphere (4% was reflected by aerosols and 16% was converted into heat that was retained within the tropospheric layers). These values are consistent with those previously calculated for the dry season in the Amazon region [*Procopio et al.*, 2004]. However, there is no data available regarding the vertical profiles associated with radiative extinction. In the present study, it was assumed that the vertical profiles for the reflection and absorption of radiation through and into the tropospheric layers by ambient biomass burning aerosols were analogous to those determined through CCN measurements taken in the field. Figure 7 shows the adjusted vertical profile used in the numerical simulations. The curve was obtained by calculating the sum of the hyperbolic and exponential functions. As suggested by the vertical CCN profiles observed during the LBA campaign [*Martins et al.*, 2004], the quantity of aerosols accumulated in the boundary layer might be a common characteristic associated with polluted conditions resulting from biomass burning in the Amazon.

4. Results

4.1. Clean Atmospheric Conditions

[23] The results obtained from the CCN300 simulation on 23 September 2002 were analyzed for grid 3. It is important to note that there is no specific arguments or data to validate the clean scenario CCN300 as the most representative. In this context, a polluted scenario could also be used as a reference. The ability of the model to accurately represent the convective activity for the simulated event can be seen in Figure 8. Figure 8a shows the topography, as well as the winds, in the first vertical layer. The spatial distribution of cloud water, as well as that of ice and rainwater (Figure 8b), the Geostationary Operational Environmental Satellite visible image (Figure 8c) and radar reflectivity (Figure 8d) are shown for 1400 LT. The selected area in Figure 8b corresponds to the fraction analyzed in all numerical simulations for grid 3. The combined results indicate that the model provides a satisfactory representation of the macroscopic properties of the weather systems on 23 September 2002.

[24] The simulated convective life cycles were found to be equivalent in duration to those observed in satellite images. The cloud cover fraction was also quite well represented. However, there was a delay in the triggering of the first convective cells. They were triggered at approximately 1200 LT in the simulations, whereas satellite images show that this occurred approximately 2 hours earlier. This delay might be related to the model spin-up, and the initialization time of the simulations appears to be a key component. According to *Meneguzzo et al.* [2004], earlier initialization can overcome the spin-up problems, although there might be a subsequent loss of predictability. Although the delay in convective activity might be related to the initial model spin-up, the model and radar data are in good agreement in terms of the life cycle of the rainwater. Therefore, the differences between the model results and observations cannot be attributed solely to the time required for model adjustment. Further improvements in the microphysical parameterization of the processes are also necessary. For example, according to BRAMS microphysics, the cloud water and rainwater parameters are activated simultaneously when the atmosphere becomes supersaturated. Obviously this is not the case in the Amazon region, where clouds appear approximately two hours before the first rain echoes are detected.

4.2. Effects of Aerosols on Convective Structures

[25] What follows is a description of the different features of the first four numerical simulations (CCN300, CCN450, CCN600 and CCN900), as well as of the radiative effects

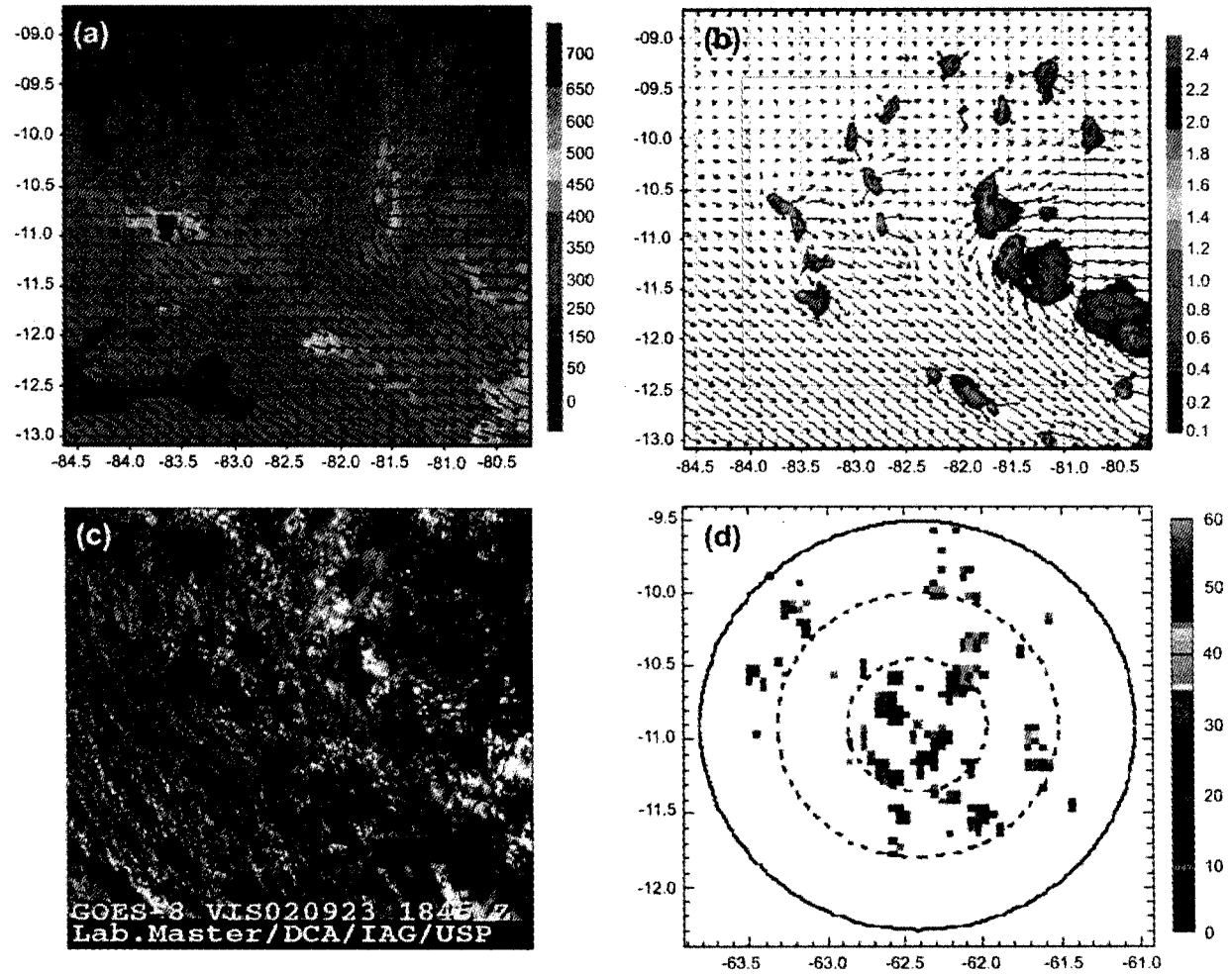

Figure 8. (a) Topography of the area (in meters), (b) simulated total water mixing ratio (in g/kg) at 600 mbar, (c) Geostationary Operational Environmental Satellite visible image showing mature convective stages, and (d) radar reflectivity (in dBZ) at the 3-km level. Fields were computed at the same time (1500 LT on 23 September 2003).

represented in scenario CCN900R. The tables summarize the main microphysical variables of interest. Cloud droplet concentration and vertical velocities refer to maximum values in space and time. Cloud cover fraction was calculated as a percentage of the total grid area occupied by any hydrometeor type. The vertically integrated ice and liquid water content (ice and liquid water paths) was calculated separately for each type, but the total water path greater than 10 g/m^2 was used as the criterion for classifying a grid point as being under cloud cover. The value was chosen just to avoid that grid points with very small not null values could be classified as covert by clouds Another small value could be also used as a criterion. However, recent analyses have demonstrated that the uncertainty associated to the remote sensing of liquid water path is between 20 and 30 g/m^2 [*Liljegren and Lesht*, 1996; *Marchand et al.*, 2003], which turn reasonable the assumed value.

[26] To describe the behavior of microphysical variables, we defined two averaged properties, both involving the water path for each hydrometeor type. The first was the spatial average-temporal average (SATA). The SATA represents a value averaged spatially and over time. Therefore, two scenarios with the same values of SATA for a given water path can present different behavior (one dominating in space and the other dominating in time). To complement this information, we defined a second property of the hydrometeors, the spatial peak-temporal average (SPTA), which corresponds to the spatial peak averaged over time. The two properties together conveniently map the microphysical evolution, in terms of space, time and intensity, under polluted conditions. The impact that aerosols have on precipitation development was analyzed according to these two integrated properties, and this analysis was extended to the ice phase, cloud water, rainwater, accumulated precipitation, cloud dynamics and surface energy balance.

4.2.1. Impact on the Ice Phase

[27] The simulation results indicate that the ice phase was quite well developed in the main cells, with high CCN concentrations (radar measurements on 23 September show deep cells reaching 16 km in height). As can be seen in Table 3, from 0.08 kg/m^2 for the clean scenario (CCN300), the ice SPTA value increased for all additional scenarios, reaching

Table 3. Ice Type Properties, Averaged Spatially and Over Time, in the Various Scenarios[a]

Microphysics Variable	Unit	CCN300	CCN450	CCN600	CCN900	CCN900R
Pristine ice SPTA	kg/m^2	0.01	0.01	0.16	0.56	0.59
Pristine ice SATA	g/m^2	0.27	0.19	0.37	2.72	2.23
Snow SPTA	kg/m^2	0.01	0.01	0.02	0.09	0.08
Snow SATA	g/m^2	0.28	0.35	0.53	2.02	1.34
Aggregates SPTA	kg/m^2	0.00	0.01	0.39	1.19	1.19
Aggregates SATA	g/m^2	0.01	0.01	0.54	7.35	6.41
Graupel SPTA	kg/m^2	0.01	0.02	0.41	1.27	1.24
Graupel SATA	g/m^2	0.00	0.01	0.66	3.18	2.78
Hail SPTA	kg/m^2	0.06	0.05	0.35	0.58	0.59
Hail SATA	g/m^2	0.19	0.02	0.56	1.06	1.02
Total ice SPTA	kg/m^2	0.08	0.10	1.34	3.70	3.69
Total ice SATA	g/m^2	0.75	0.58	2.66	16.34	13.79

[a]CCN, cloud condensation nuclei; CCN300, scenario representing "clean" conditions (CCN concentration, 300 cm^{-3}); CCN450, scenario representing "relatively clean" conditions (CCN concentration, 450 cm^{-3}); CCN600, scenario representing "moderately polluted" conditions (CCN concentration, 600 cm^{-3}); CCN900, scenario representing "polluted" conditions (CCN concentration, 900 cm^{-3}); CCN900R, scenario also representing "polluted" conditions (CCN concentration, 900 cm^{-3}) but with radiative forcing; SATA, spatial average-temporal average; SPTA, spatial peak-temporal average.

3.7 kg/m^2 for scenarios CCN900 and CCN900R. The corresponding SATA values presented a different behavior, that obtained for scenario CCN450 actually being lower than that obtained for scenario CCN300, and all remaining scenarios presenting increases in the SATA that were less pronounced than the increases in the SPTA. For scenario CCN900, the SPTA was 45 times greater than that obtained for scenario CCN300, whereas the SATA was only 16 times greater (the radiative effect attenuated only the SATA). Under clean or relatively clean conditions (CCN300 and CCN450), the SPTA was dominated by hail, whereas it was dominated by aggregates, graupel and hail under moderately polluted conditions (CCN600), and by aggregates and graupel under polluted conditions (CCN900 and CCN900R). For all ice types, the SATA presented similar evolution under moderately polluted conditions (CCN600) but was dominated by aggregates under polluted conditions (CCN900 and CCN900R).

[28] In the simulations, the full development of convective cells promoted the production of great quantities of ice. Primary ice processes were modeled, as were secondary ice processes. The total temporal evolution of the ice water path for all simulations is shown in Figure 9. Mean values presented behavior similar to that of maximum values. On the basis of the results of the simulations, it seems that the impact of CCN on ice phase development peaks at a certain CCN concentration. However, when radiative effects are included (scenario CCN900R), there is a delay in the beginning of the ice phase. Higher CCN concentrations increase the quantity of ice, although this effect is smoothed by the superposition of the radiative effects. The results suggest that aerosols, whether acting as CCN or providing radiative forcing, modify not only the intensity but also the spatiotemporal aspects of ice-phase distribution. However, maximum values correlate quite well with mean values for all scenarios. Since the total quantity of ice is significantly greater only at high CCN concentrations (Table 3), the SATA and SPTA values suggest that the increase in the ice water path is caused by aggregates and graupel, pristine ice, snow and hail making smaller contributions. These findings are consistent with those of *Lin et al.* [2006], who observed an increase in high-level cloud cover and reduction of cloud top temperature with increased aerosol optical depth, which is coherent with the results of the present simulations.

[29] In the BRAMS model, separate analysis allows the size distribution of ice crystals to be characterized in a

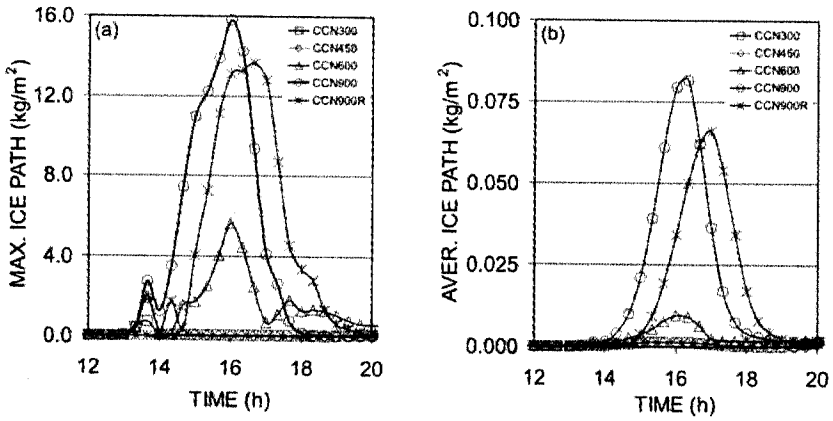

Figure 9. (a) Maximum and (b) mean temporal evolution of the ice water path in the various simulated scenarios. CCN, cloud condensation nuclei; CCN300, CCN concentration for 300 cm^{-3}; CCN450, CCN concentration for 450 cm^{-3}; CCN600, CCN concentration for 600 cm^{-3}; CCN900, CCN concentration for 900 cm^{-3}; CCN900R, CCN concentration for 900 cm^{-3} with radiative forcing; MAX., maximum.

bimodal manner: relatively large crystals (formed by vapor deposition and riming) are categorized as snow, and smaller crystals (formed by vapor deposition alone) are categorized as pristine ice. The clean and relatively clean scenarios produced smaller quantities of ice. However, in those same scenarios (CCN300 and CCN450), the life cycle of ice crystals was longer than that of other ice types. Most of that difference was attributable to changes in the SATA; in terms of the SPTA, there was no clear trend. These differences were found for both types of ice crystals. In scenario CCN900R, the ice type most affected by radiative effects was snow crystals, the SPTA for which was reduced by more than 30%. The overall pattern of the ice phase during the simulations indicates that ice types are sensitive to CCN concentration and radiative forcing, the former having the greater impact.

[30] Clouds that form in polluted environments have been shown to contain droplets that are greater in number but smaller in size. Such clouds present low efficiency in producing precipitation via the collision-coalescence process. However, our numerical results indicate that, in convective clouds such as those observed in the Amazon region and simulated in the present study, aerosol-induced suppression of warm rain can be overpowered by a change in the predominant pattern, at least in the core of the convective systems. Homogeneous freezing might be less likely under polluted conditions, owing to the smaller size of the cloud droplets. However, in deep convective clouds with warm bases, greater droplet numbers and smaller droplet size, although delaying precipitation, might cause the droplets to ascend to the higher, supercooled levels. The additional vertical decrease in temperature to which the cloud droplets would be exposed might compensate for the reduced efficiency in freezing. The Bergeron process might also being intensified by the increased availability of cloud droplets at the upper levels.

[31] Additional aerosol effects on the ice phase include soot particles functioning as ice nuclei. This could increase the numbers and decrease the size of ice crystals, thereby promoting heterogeneous freezing or even decreasing collection. In addition, the possibility that some particles might be coated with soluble compounds that could reduce ice nuclei numbers and increase the numbers of CCN was not included in the scenarios. Therefore, it remains unknown whether this factor would have an impact on precipitation development in the scenarios simulated.

4.2.2. Impact on Cloud Water and Rainwater

[32] As indicated in Table 4, the maximum cloud droplet concentration varied from 64 to 72% of the CCN concentration. The maximum activated values were 192, 296, 424, 646 and 641 cm^{-3} for scenarios CCN300, CCN450, CCN600, CCN900 and CCN900R, respectively. The fraction of activated CCN was higher in the moderately polluted and polluted scenarios than in the clean and relatively clean scenarios. The cloud water SPTA during the simulation increased in parallel with the CCN concentration and was 2.66 times greater in scenario CCN900 than in scenario CCN300, although it was only 2.44 times greater in scenario CCN900R, indicating an attenuation effect. The SATA values presented a trend opposite that observed for the SPTA values. The SATA values for scenarios CCN450, CCN600, CCN900 and CCN900R were found to be approximately 13, 5, 19 and 20% lower, respectively, than those obtained for scenario CCN300. In terms of absolute values, the cloud water SATA was less affected than was the cloud water SPTA. In addition, the decrease in SATA values presented no regular pattern. This implies that pollution can also increase cloud water, since SATA values were higher for scenario CCN600 than for scenario CCN450. The trend in cloud water values was found to be dependent on the profile of the reference scenario chosen to represent "clean" conditions.

[33] Comparing the moderately polluted and polluted scenarios with the cleanest scenario, rainwater SPTA values were more than 2 times greater, whereas rainwater SATA values were lower (33, 26, 43 and 40% lower for scenarios CCN450, CCN600, CCN900 and CCN900R, respectively, than for scenario CCN300). According to the numerical results, the SPTA and SATA were both affected by pollution, and the greatest differences were found for the polluted scenarios (CCN900 and CCN900R). Rainwater was weakly influenced by the aerosol radiative effect, only slight increases being seen in the rainwater SPTA and SATA values. It is noted that there was a complex effect involving the different scenarios. Using scenario CCN300 as a reference, scenario CCN450 presented no significant difference in terms of the SPTA, although the SATA was markedly lower. However, if scenario CCN450 were used as the reference scenario representing clean conditions, the rainwater SPTA for scenario CCN600 would be significantly greater, and there would be no significant difference in terms of SATA.

4.2.3. Impact on Total Accumulated Precipitation and Cloudiness

[34] The sum of different condensed water types represents the vertically integrated ice and liquid water content, which defines the patterns of observed accumulated surface precipitation. There was no observation of any ice precipitation at surface. As can be seen in Table 5, the SPTA values for the vertically integrated ice and liquid water content were 2.96, 3.22, 7.01, 9.25 and 9.35 kg/m^2 in scenarios CCN300, CCN450, CCN600, CCN900 and CCN900R, respectively. The corresponding SATA values were 115.6, 90.5, 101.1, 97.0 and 95.2 g/m^2. In terms of the vertically integrated ice and liquid water content, it appears that an increase in CCN concentration has the potential to increase the SPTA. However, SATA values can increase or decrease, depending on the CCN concentration chosen to represent clean conditions. For example, if CCN450 is used as a polluted scenario in relation to CCN300, the higher CCN concentration causes a reduction in the SATA, whereas, if CCN600 is used as a polluted scenario in relation to CCN450, the higher CCN concentration causes an increase in the SATA.

[35] The evolution of maximum rainfall rate roughly follows the trend identified for the vertically integrated ice and liquid water content. As shown in Figure 10, the maximum rainfall rate found for scenario CCN900 was approximately 57.8 mm/h. The clean and relatively clean scenarios were characterized by low maximum rainfall rates. The maximum rainfall SPTA values were 5.0, 5.4, 15.6, 19.3 and 20.2 mm/h for scenarios CCN300, CCN450, CCN600, CCN900 and CCN900R, respectively. The corresponding values of SATA were 0.126, 0.091, 0.134, 0.119 and 0.125 mm/h.

[36] The highest accumulated precipitation value was found for scenario CCN900R (100.9 mm), followed by scenarios CCN900 (87.7 mm), CCN600 (53.7 mm), CCN450 (22.2 mm) and CCN300 (16.9 mm). The grid-

Table 4. Cloud Water and Rainwater Type Properties, Averaged Spatially and Over Time, in the Various Scenarios[a]

Microphysics Variable	Unit	CCN300	CCN450	CCN600	CCN900	CCN900R
Maximum cloud droplet concentration	cm^{-3}	192	296	424	646	641
Cloud water SPTA	kg/m^2	1.01	1.29	2.29	2.69	2.48
Cloud water SATA	g/m^2	64.60	56.27	61.45	52.06	51.36
Rainwater SPTA	kg/m^2	1.95	1.93	4.22	4.90	4.95
Rainwater SATA	g/m^2	50.22	33.68	36.97	28.60	30.11

[a]CCN, cloud condensation nuclei; CCN300, scenario representing "clean" conditions (CCN concentration, 300 cm^{-3}); CCN450, scenario representing "relatively clean" conditions (CCN concentration, 450 cm^{-3}); CCN600, scenario representing "moderately polluted" conditions (CCN concentration, 600 cm^{-3}); CCN900, scenario representing "polluted" conditions (CCN concentration, 900 cm^{-3}); CCN900R, scenario also representing "polluted" conditions (CCN concentration, 900 cm^{-3}) but with radiative forcing; SATA, spatial average-temporal average; SPTA, spatial peak-temporal average.

averaged values presented a different trend, the highest value being found for scenario CCN600 (1.03 mm), followed by scenarios CCN900R (0.99 mm), CCN300 (0.96 mm), CCN900 (0.94) and CCN450 (0.69 mm). These results suggest that the presence of aerosols acting as CCN favors the occurrence of more intense precipitation cores at any elevated level of pollution (Figure 11a). However, the mean values were either reduced or increased, depending on the level of pollution (Figure 11b). The full development of the cold phase can play a significant role in the partitioning among hydrometeor types, as well as in defining the vertically integrated ice and liquid water content and accumulated precipitation.

[37] On the basis of the physical interpretation of the modeling used herein, higher CCN concentrations, together with the corresponding shape parameters, slow the autoconversion of cloud water into rainwater. Since small cloud droplets fall slower than do larger droplets, higher CCN concentrations suppress warm rain. Empirical evidences of aerosols inhibiting rainfall were presented earlier by *Rosenfeld and Lensky* [1998], *Rosenfeld* [1999, 2000], *Toon* [2000] and *Ackerman et al.* [2003]. As a consequence of the aerosol suppressing effect, an opposing force can appear. The high concentration of small cloud droplets, which are slow to coalesce into raindrops, also intensifies the latent heat released during the freezing process, which in turn accelerates the rising currents of air within clouds. These updrafts can intensify and redistribute the water within the convective cells, transforming the warm rain process into a cold rain process. However, smaller cloud droplets could likely evaporate more than larger ones, so as this process could compete with the buoyancy effect caused by the latent heat release, mainly in the small convective cells. Aerosol dynamic effects on convective clouds, as those discussed in this work, were also pointed by a number of previous works [*Khain et al.*, 2003; *Khain and Pokrovsky*, 2004; *Khain et al.*, 2005; *Lynn et al.*, 2005a, 2005b; *Phillips et al.*, 2007, *Tao et al.*, 2007; *Lee et al.*, 2008].

[38] The results of the numerical simulations run in the present study indicate that total precipitation can increase or decrease, depending on the level of pollution used in the reference scenario. The most important question here is whether aerosol-cloud-precipitation interactions produce predictable effects. Figure 12 shows the partitioning of rainfall rates (RR) in terms of the SATA for different ranges. The SATA can be seen as an evaluation of the overall (grid) contribution of each scenario. In order to evaluate the contribution of different rainfall rates (RR) on SATA values, the RR, expressed in units of mm/h, were converted into three classes as shown by the Figure 12: RR < 1 mm/h (low RR), 1 mm/h $\leq$ RR < 5 mm/h (moderate RR) and RR $\geq$ 5 mm/h (high RR). The results show that the increase in CCN concentration reduce the contribution of low and moderate RR over the grid area. However, high RR are increased by the increase in CCN concentrations. It is noted that, in the scenario representing moderate pollution (scenario CCN600), the decrease in low RR was not significantly affected, whereas high RR was increased. This particular behavior can explain, in part, why aerosols can either increase or decrease precipitation, depending on the level of CCN concentration taken as representative of 'clean' conditions. As reported by *Lin et al.* [2006], increased pollution primarily results in a change in the probability density function of the rainfall rate with no clear impact on the total averaged accumulated surface precipitation.

[39] According to our results, high CCN concentrations can potentially decrease total cloudiness. Polluted scenarios

Table 5. Total Quantity of Vertically Integrated Water, Accumulated Precipitation, and Cloudiness, Averaged Spatially and Over Time, in the Various Scenarios[a]

Microphysics Variable	Unit	CCN300	CCN450	CCN600	CCN900	CCN900R
Total water SPTA	kg/m^2	2.97	3.23	7.01	9.25	9.35
Total water SATA	g/m^2	115.57	90.53	101.08	97.00	95.25
Rainfall rate SPTA	mm/h	4.97	5.44	15.57	19.34	20.17
Rainfall rate SATA	mm/h	0.13	0.09	0.13	0.12	0.13
Maximum accumulated precipitation	mm	16.94	22.15	53.74	87.66	100.88
Mean accumulated precipitation	mm	0.96	0.69	1.03	0.94	0.99
Maximum cloud cover	%	33.28	27.97	24.01	18.97	17.59
Max. ice cover	%	0.11	0.14	2.60	10.49	6.35
Maximum vertical velocity	m/s	2.25	2.39	5.16	7.83	8.37
Surface energy gain	MJ/m^2	1.38	1.57	1.63	1.75	1.52

[a]CCN, cloud condensation nuclei; CCN300, scenario representing "clean" conditions (CCN concentration, 300 cm^{-3}); CCN450, scenario representing "relatively clean" conditions (CCN concentration, 450 cm^{-3}); CCN600, scenario representing "moderately polluted" conditions (CCN concentration, 600 cm^{-3}); CCN900, scenario representing "polluted" conditions (CCN concentration, 900 cm^{-3}); CCN900R, scenario also representing "polluted" conditions (CCN concentration, 900 cm^{-3}) but with radiative forcing; SATA, spatial average-temporal average; SPTA, spatial peak-temporal average.

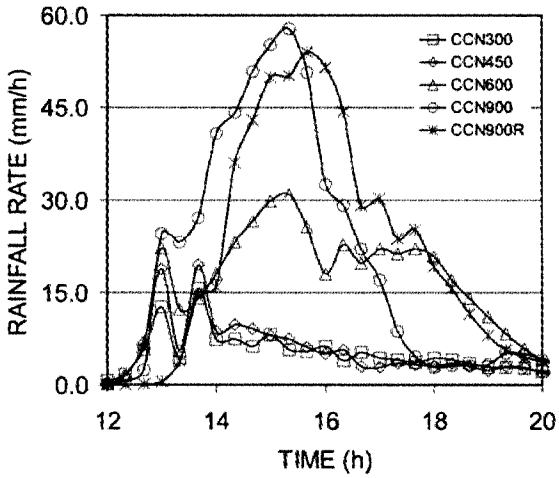

Figure 10. Temporal evolution of rainfall rates in terms of maximum values in the grids. CCN, cloud condensation nuclei; CCN300, CCN concentration for 300 cm^{-3}; CCN450, CCN concentration for 450 cm^{-3}; CCN600, CCN concentration for 600 cm^{-3}; CCN900, CCN concentration for 900 cm^{-3}; CCN900R, CCN concentration for 900 cm^{-3} with radiative forcing.

presented a reduction in cloud cover of more than 30% in relation to scenario CCN300. This is a finding that is in accordance with observations, based on shallow cumulus fields, made by *Koren et al.* [2004]. The simulations run by those authors showed that aerosols, at any level of pollution, diminish the cloud cover fraction, which is dominated by the shallow cloud fraction. However, in our simulated results, the reduction might be accompanied by a vertical increase in the ice water path. As a consequence, upper-level cloud cover could also increase. The overall effect is that, under polluted conditions, cloudiness is less dispersed, and there is a significant reduction in low-level cloudiness. In the present study, this less dispersed pattern was slightly more pronounced when radiative effects were assumed to occur concurrently with an increase in CCN concentration (scenario CCN900R).

[40] By absorbing radiation, certain aerosols can modify the thermal structure of the atmosphere and the surface energy balance. The accumulation of such aerosols in the lower layers of the atmosphere leads to atmospheric warming, which can suppress small-scale convection, thereby reducing cloudiness and precipitation. Although cloudiness was approximately 7% lower in scenario CCN900R than in scenario CCN900, we do not know whether that reduction is attributable to the absorbing aerosols alone.

4.2.4. Impact on Cloud Dynamics

[41] The maximum updrafts were stronger in the moderately polluted and polluted scenarios than in the clean scenario. Vertical velocities were 8.4 m/s in scenario CCN900R, 7.8 m/s in scenario CCN900, 5.2 m/s in scenario CCN600, 2.4 m/s in scenario CCN450 and 2.3 m/s in scenario CCN300. Figure 13 presents the temporal evolution of the updrafts and downdrafts in all numerical simulations. Maximum downdraft values, although lesser in magnitude than the maximum updraft values, were greater for the moderately polluted and polluted scenarios than for the clean scenario. Apparently, aerosols can significantly modify the dynamic structure of the precipitation process, in agreement with previous results found by *Khain et al.* [2003], *Khain and Pokrovsky* [2004], *Khain et al.* [2005], *Lynn et al.* [2005a, 2005b], *Phillips et al.* [2007], *Tao et al.* [2007], and *Lee et al.* [2008].

[42] All simulations involving higher CCN concentrations presented increases in the maximum values for cloud water and rainwater. These increases were restricted to the core of well-developed convective cells. We can suppose that this is a consequence of the greater buoyancy related to the large number of droplets, which alters the distribution of water. The changes in the distribution of buoyancy, caused by the modification of the microphysical paths, also influenced the vertical velocity components. In addition, the vertical structure of the cloud water and ice water paths indicates that cloud tops are higher in moderately polluted and polluted scenarios than in clean scenario (Figure 14). Therefore, after

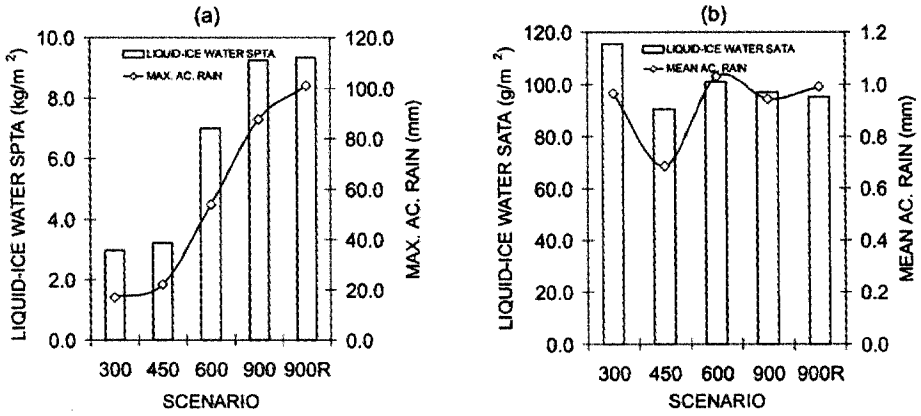

Figure 11. Simulated changes in vertically integrated ice and liquid water and surface accumulated precipitation in terms of (a) maximum and (b) mean values. SATA, spatial average-temporal average; SPTA, spatial peak-temporal average; MAX., maximum; AC., accumulated; 300, "clean" conditions; 450, "relatively clean" conditions; 600, "moderately polluted" conditions; 900, "polluted" conditions; 900R, "polluted" conditions with radiative forcing.

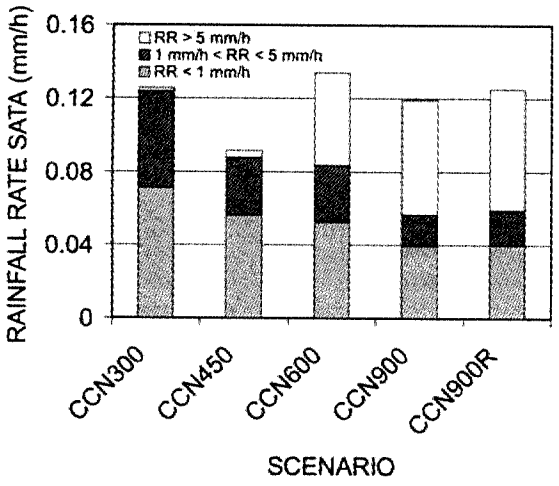

Figure 12. Partitioning of the rainfall rate SATA, expressed in units of mm/h, into three classes: RR < 1 mm/h; 1 mm/h ≤ RR < 5 mm/h; and RR ≥ 5 mm/h. RR, rainfall rate; SATA, spatial average-temporal average; CCN, cloud condensation nuclei; CCN300, CCN concentration for 300 cm^{-3}; CCN450, CCN concentration for 450 cm^{-3}; CCN600, CCN concentration for 600 cm^{-3}; CCN900, CCN concentration for 900 cm^{-3}; CCN900R, CCN concentration for 900 cm^{-3} with radiative forcing.

a minimum level of ice concentration has been reached, an increase in CCN concentration invigorates cloud cells and produces large amounts of ice. This can be understood as a dynamic effect in which excess latent heat released during the freezing process causes vertical updraft velocities to be greater than those obtained for warm rain processes, in agreement with the above-mentioned previous studies.

4.2.5. Impact on Energy Balance

[43] As previously discussed, when CCN concentrations are higher (as in scenarios CCN600 and CCN900), water is concentrated in a few intense convective cells. In such scenarios, this change in convection was evidenced by the fact that cloud formation was more vigorous than that modeled in the clean scenario, and that the corresponding cloud tops reached higher elevations. One direct consequence was a reduction in cloudiness, which increased the amount of solar radiation reaching the boundary layer and surface. As might be expected, this changed the surface latent heat flux, sensible heat flux and long-wave radiative flux. A similar effect could be expected for scenario CCN900R. However, in that case, aerosol particles exerted a direct effect, reducing the incoming solar radiation received by the surface, at least prior to cloud formation.

[44] Figure 15 represents the net relative surface energy (latent heat flux, sensible heat flux, short-wave radiative flux and long-wave radiative flux). Positive values indicate that there was a greater amount of solar radiation reaching the surface, in comparison with the clean scenario. By comparing the curves, it can clearly be seen that, in the moderately polluted and polluted scenarios, there was a greater amount of solar radiation reaching the surface in the periods during which the convective events were more intense. The negative radiative flux predominating during the periods of dissipation are equally obvious. In scenario CCN900R, the negative values predominating during the period prior to the triggering of convection are attributable to direct absorption or reflection by aerosols. The overall net surface energy balance during the 24-h simulation was 1.38, 1.57, 1.63, 1.75 and 1.52 MJ/m^2 for scenarios CCN300, CCN450, CCN600, CCN900 and CCN950R, respectively. Therefore, surface energy budgets were higher in the moderately polluted and polluted scenarios.

[45] Assuming that scenario CCN900R is more realistic than the scenarios in which aerosols only increase CCN concentrations (scenarios CCN450, CCN600 and CCN900), either positive or negative net surface energy gains are possible. Aerosols can either heat or cool the surface depending on their chemical composition and vertical distribution. If the particles are more effective as CCN than as radiation absorbers, the net effect is heating. However, if the inverse is true, the net effect is cooling. In scenario CCN900R, the result was surface heating, although it was less intense than

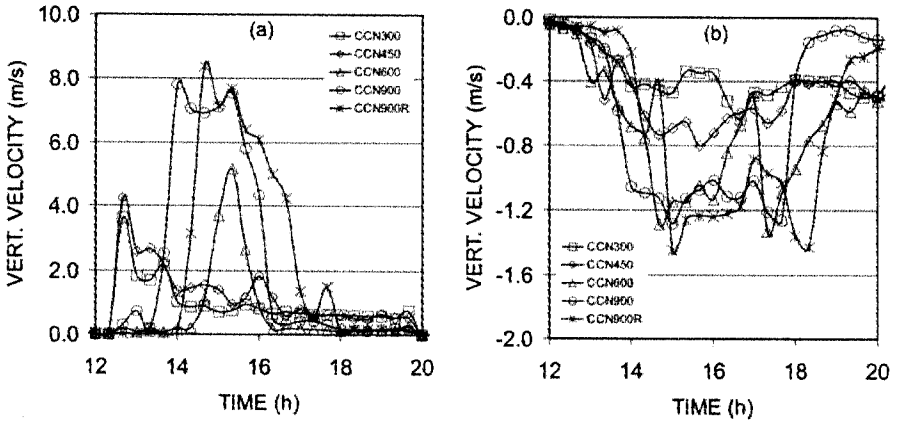

Figure 13. Temporal evolution of the maximum (a) updraft and (b) downdraft observed in the five simulated scenarios. VERT, vertical; CCN, cloud condensation nuclei; CCN300, CCN concentration for 300 cm^{-3}; CCN450, CCN concentration for 450 cm^{-3}; CCN600, CCN concentration for 600 cm^{-3}; CCN900, CCN concentration for 900 cm^{-3}; CCN900R, CCN concentration for 900 cm^{-3} with radiative forcing.

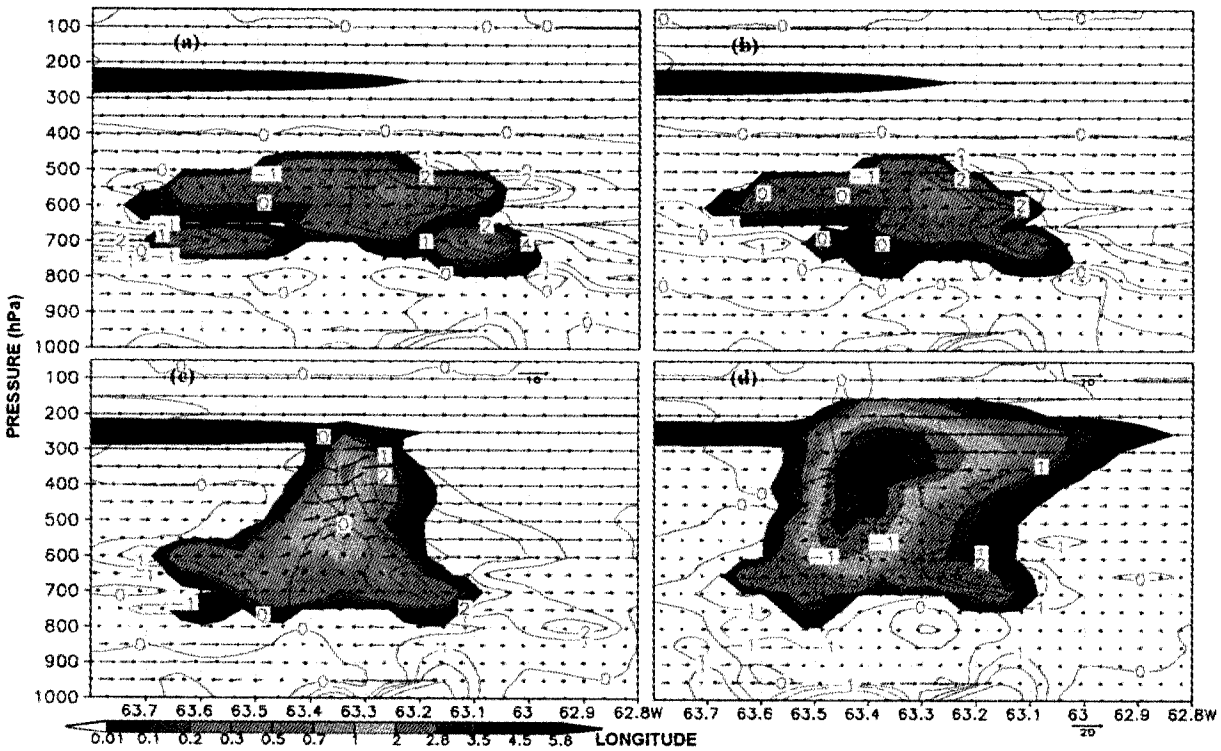

Figure 14. Vertical structure of cloud and ice water mixing ratio (g/kg) observed at the time of maximum liquid water path for a typical convective cell in the scenarios (a) CCN300, (b) CCN450, (c) CCN600, and (d) CCN900. Contour lines represent the vapor mixing ratio temporal evolution (g/kg/h). CCN, cloud condensation nuclei; CCN300, CCN concentration for 300 cm^{-3}; CCN450, CCN concentration for 450 cm^{-3}; CCN600, CCN concentration for 600 cm^{-3}; CCN900, CCN concentration for 900 cm^{-3}.

that seen in the other scenarios. A scenario such as CCN900R could certainly cause surface cooling. Therefore, it is likely that certain situations lead to a nonpredictable effect, in which biomass burning aerosols could promote surface heating or cooling depending on how efficient the aerosols are in terms of their hygroscopic and radiative properties.

[46] The atmospheric heating associated with the radiative effect of aerosols, such as that seen in scenario CCN900R, can profoundly influence vertical temperature distribution and atmospheric stability. First, as shown in Figure 7, aerosol-related heating is greater within the boundary layer, increasing the vertical temperature gradient, which can increase vertical velocities. Another effect is attributed to the sensible heat flux at the surface, the transfer of sensible heat being strongly influenced by the temperature difference between the surface and the ambient air. As a consequence, the lower layers of the atmosphere were warmer in scenario CCN900R than in scenario CCN300, and the surface was cooler. Therefore, it would be reasonable to assume that the sensible heat flux is reduced as a direct consequence of aerosol absorption of radiation. The lower surface temperature might also explain the relatively lower latent heat flux (net gain) seen in scenario CCN900R. These mechanisms might be responsible for the increase in the surface net energy in the afternoon of scenario CCN900R (Figure 15).

[47] The results of the numerical simulations, which reveal direct, semidirect and indirect effects, must be considered

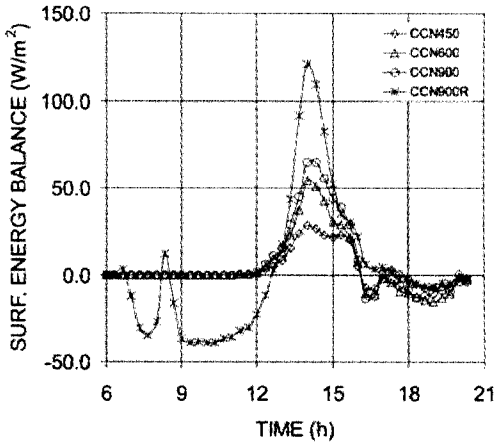

Figure 15. Temporal evolution of the relative surface energy balance. The net energy for the relatively clean, moderately polluted, and polluted scenarios was calculated in comparison to that obtained for the clean scenario, in which the cloud condensation nuclei (CCN) concentration was set at 300 cm^{-3} and which was taken as 0.0 W/m^2. Positive values indicate net surface energy gain. SURF., surface; CCN450, CCN concentration for 450 cm^{-3}; CCN600, CCN concentration for 600 cm^{-3}; CCN900, CCN concentration for 900 cm^{-3}; CCN900R, CCN concentration for 900 cm^{-3} with radiative forcing.

hypothetical. However, empirical evidence should support our finding that the microphysical effects of aerosols included suppression/promotion of convection and modification of the surface energy balance. In particular, our finding that high black carbon concentrations reduced total radiation at the surface should be interpreted with caution, since there are limitations in our model as it does not describe the aerosols as they are. The role that black carbon plays in increasing or reducing cloudiness, with the corresponding consequences for net surface energy, remains unclear. Nevertheless, this finding is particularly important because it lends credence to the idea that the biomass burning-related increase in CCN concentrations is directly associated with the concurrent increase in the concentration of black carbon, each having its own unique impact on surface energy partitioning. If, as suggested by the aerosol effects presented herein, black carbon and CCN are spatially correlated, then, within the context of the effect of biomass burning, the two are in competition, the former decreasing and the latter increasing the amount of solar radiation reaching the surface.

5. Conclusions

[48] Five numerical simulations were run for the southwestern Amazon region in order to examine the spatial and temporal effects that atmospheric aerosols have on cloud microphysics and accumulated precipitation. The mechanism by which aerosols affect precipitation structure was investigated by examining the correlations between CCN concentrations and changes in precipitation variables. According to empirical evidence, CCN concentrations are associated with the shape parameters of cloud droplets. The aerosol radiative effect on tropospheric air was also considered in the numerical simulations, and the precipitation properties changed significantly. In regional modeling, higher aerosol concentrations tend to have a significant impact on the spatial and temporal dimensions of the precipitation process, increasing the importance of aerosol effects in the dynamics of the cloud-precipitation systems. The sensitivity of the precipitation process to the CCN concentration appears to be highly complex: areas of higher CCN concentration presenting increases in total precipitation can coexist with those presenting decreases in total precipitation.

[49] The hydrological cycle can be strongly affected by alterations in CCN concentration, which can result in changes in the quantity of cloud water and in precipitation rates. Higher concentrations of anthropogenic aerosols, and consequently of CCN, decrease cloud droplet size, which might reduce the amount of accumulated precipitation at the edge of convective cells, since smaller droplets are less likely to collide and to form precipitation (the warm rain process). However, the intensification of the ice phase increases precipitation within such cells. Primary and secondary ice-nucleation parameterizations represented in the BRAMS cloud module might have implications for the spatial and temporal distribution of precipitation. High CCN concentrations have significant effects on the microphysics and dynamics of mixed-phase clouds, not only by modifying warm rain in the lower portions of the cloud but also by interacting with the ice phase. One limitation of the present study was that radiative effects were examined in a simple way. The first indirect effect, in which a greater number of smaller cloud droplets present an increase in surface area, and therefore reflect more sunlight, was not evaluated.

[50] The numerical results indicate that, when CCN concentrations are high, the hydrological cycle, assessed in terms of the mean values for water types, can be accelerated or decelerated. However, in simulations assuming a high CCN concentration, the maximum values increased for all water types. A delay in the triggering of convection, together with reductions in the life cycle and horizontal dimension of convective cells, revealed that higher aerosol concentrations have temporal and spatial effects. The mean liquid water path was found to decrease in parallel with increases in pollution, although the pattern identified for warm-phase processes was distinct from that identified for mixed-phase processes. Maximum values for the liquid water path always increased in parallel with increases in pollution. The ice water path showed a general shift to higher values as pollution levels increased. In addition, vertical updrafts and downdrafts were stronger in moderately polluted and polluted scenarios, in agreement with previous numerical studies. The aerosol effect of blocking radiation by absorption and reflection tended to smooth the effects of CCN concentration on microphysical properties. The effect was found for cloud water and ice but not for rainwater, the last presenting an increase.

[51] Although there is a large body of data related to the effects of aerosols on precipitation, only a few studies have employed atmospheric models including detailed microphysics. Bulk parameterization and spectral microphysics are typically used in order to represent the precipitation process. There have been even fewer regional modeling studies focusing on deep convective clouds, and the results of those studies are similar to those presented here in many aspects but different in others.

[52] *Reisin et al.* [1996] performed simulations of cloud seeding with ice nuclei and hygroscopic particles using a numerical model with detailed treatment of both warm and cold microphysical processes. The seeding time was found to be a critical parameter for obtaining positive results. The optimal "time window" for IN seeding was found to be very short and to correspond to the time at which the natural ice began to form. Seeding after this time reduced the rain. In the maritime clouds, rain formation processes were very efficient, and seeding did not produce any significant increase in rain amounts. In the moderate and extreme continental clouds, seeding with IN at the optimal time and location increased the precipitation by 9% and 35%, respectively. Rainfall did not change with the seeding of IN in the warmer cloud with a top temperature of $-12°C$. Seeding with hygroscopic particles caused a increases of 65% and 109% in rain amounts for the moderate and extreme continental clouds, respectively. In these cases, the optimal time window was longer, and even clouds with tops at $-12°C$ doubled their rain amounts.

[53] Using numerical experiments, *Teller and Levin* [2006] investigated the effects of increased concentrations of CCN, giant CCN and IN on the development of precipitation and cloud structure in mixed-phase subtropical convective clouds. Their results showed that under the same meteorological conditions, polluted clouds (with high CCN concentrations) produce less precipitation than clean clouds (with low CCN concentrations). In addition, the initiation of

precipitation is delayed and the lifetimes of the clouds are longer. Giant CCN enhance the total precipitation in polluted clouds but not in cleaner clouds. The addition of more effective IN, such as mineral dust particles, reduces the total amount of precipitation on the ground. This reduction was observed to be more pronounced in clean clouds than in polluted ones. Polluted clouds reach higher altitudes and are wider than clean clouds and both produce wider clouds (anvils) when more IN are introduced.

[54] The above two works corroborate the complexity involving the aerossol-precipitation interactions and the role of the nonmicrophysical actors involved in the precipitation development. Their results also emphasize the importance associated to the increase in the giant CCN and IN concentrations, not discussed in this work.

[55] The effects that different CCN size distributions have on the evolution of deep convective clouds under dry unstable continental thermodynamic conditions were investigated by *Khain and Pokrovsky* [2004] using the spectral microphysics Hebrew University Cloud Model. According to the authors, the numerical simulations indicated a significant decrease in accumulated precipitation in smoky air. However, the fraction of total precipitation attributed to warm rain was low in smoky continental air and dominated in clean maritime air. Since warm rain accounts for a smaller fraction of total precipitation, the lower quantity of accumulated rain in smoky air can be primarily attributed to the reduction in the amount of melted precipitation. *Khain et al.* [2005], using the same spectral microphysical cloud model, simulated maritime and continental-type scenarios. They observed that the increase in aerosol concentration influences the precipitation type, promoting the formation of ice precipitation and decreasing the warm rain amount. The results of simulations also showed that the cloud lifetime, as well as the area covered by clouds, increase with the increase in CCN concentration. The authors suggested that aerosols can contribute to the formation of very intensive convective structures accompanied by very high precipitation rates. The mechanism by which the storm is intensified is the additional latent heat release by the condensation and freezing of water that rises to the freezing level. The present results can also confirm those ones from *Khain et al.* [2005], such as a delay in precipitation onset, reduction of the warm rain precipitation at the ground and larger updrafts. By considering the deepest convective cells, we can also confirm the increase in area covered by clouds (see maximum ice cover in Table 5).

[56] In a study conducted by *van den Heever et al.* [2006], the impact that higher concentrations of aerosols have on the characteristics of convective storms and their subsequent anvil development was evaluated using a version of the RAMS model. Initialization profiles of CCN, giant CCN and ice nuclei concentrations were used. Variations in the initialization profiles were found to have significant effects on storm dynamics and microphysical processes, as well as on surface precipitation. Updrafts were found to increase in strength as aerosol concentrations increased. Cloud water mass increased in parallel with increases in aerosol concentrations, with the giant CCN concentrations having the most significant influence. Increasing the concentration of giant CCN or of ice nuclei resulted in greater amounts of rainfall at the surface, which was reduced when CCN concentrations were increased. In contrast to the BRAMS model, the version of RAMS employed by those authors included an additional giant CCN mode. Despite the difference between our model versions, the much more vigorous convection under high CCN concentration and the increase in cloud water path are similar conclusions.

[57] Using the abovementioned version of RAMS, *van den Heever and Cotton* [2007] investigated the impacts of urban-enhanced aerosol concentrations on convective storm development and precipitation over and downwind of St. Louis, Missouri. The results indicated that urban-forced convergence downwind of the city, rather than the presence of higher aerosol concentrations, determined whether storms actually developed in the downwind region. However, the authors also showed that, after convection has begun, urban-enhanced aerosol concentrations can exert a significant effect on the rate and amount of liquid water and ice produced, as well as on accumulated surface precipitation and storm dynamics. As in our study, complex relationships and feedbacks were found between the microphysics and storm dynamics, making it difficult to draw definitive conclusions regarding the effects of urban-enhanced aerosol concentrations on downwind precipitation and convection. Those authors found that, at higher CCN concentrations, updrafts strengthened, which in turn deepened the storm system. Another interesting aspect is that, in the simulations from which the urban region was excluded, storms did not develop in the vicinity of the city, even if the urban-enhanced aerosol concentration were maintained in the region. Although we did not run similar tests, the results obtained by those authors suggest that, in the present study, local topography influenced the triggering of the storms downwind of the more elevated areas.

[58] *Lynn et al.* [2005a] implemented a spectral bin microphysics parameterization in the MM5 mesoscale model. According to the authors, the cloud structure modeled thus was more realistic than that obtained with the bulk parameterization employed in the MM5 model. Using the new implemented version, the authors simulated a squall line that developed over Florida on 27 July 1991 [*Lynn et al.*, 2005b]. They found that an increase in precipitation was found only in zone of deep convection, while a very small decrease in precipitation over the entire computational domain was reported. So, the results of the present study agree well with those obtained by *Lynn et al.* [2005b], underscoring the idea that aerosols tend to intensify deep convection and to decrease precipitation from lower clouds.

[59] Using a three-dimensional cloud-resolving model, *Wang* [2005] studied the ways in which the cloud physical processes of a developing tropical deep convection respond to increases in CCN concentration. The study showed that higher CCN concentrations increase cloud cover and precipitation. This is a result that corroborates our work when observing properties concerning the deepest convective cells. In addition, the authors showed that the effects were insignificant when the initial CCN concentration exceeded a certain level.

[60] Using a two-dimensional cloud resolving model, idealized low and high CCN conditions were simulated by *Tao et al.* [2007] in three distinct regions. Rain suppression and delay in the precipitation is evident in all three cases with high CCN concentration. However, the suppression was observed to occur only during the early stages of the

simulations. During the mature stages of the simulations the effects of increasing aerosol concentration varied from rain suppression to rain enhancement, depending on the region analyzed.

[61] A minor number of recent studies involving numerical simulations have focused on the effects that aerosols have on precipitation development in warm cumulus clouds [*Xue and Feingold*, 2006; *Jiang and Feingold*, 2006; *Jiang et al.*, 2006; *Altaratz et al.*, 2008]. A set of cloud properties were investigated, as was accumulated surface precipitation, and the results varied among the studies. Nevertheless, the results of those studies suggest that, in small clouds, evaporation plays a key role in determining how cloud properties respond to an increase in aerosol concentration.

[62] Although the simulations run by many above mentioned authors were not identical to ours in context (different regions, atmospheric conditions, physical parameterizations, resolutions), most of their findings confirm our results, in special those concerning deep convection. In attempting to answer questions regarding the anthropogenic effects that certain factors have on climate, we should recognize the natural physical complexity of the atmosphere. The present study had various limitations. Of course, the physics of aerosol-rain interaction is much more complicated than can be described through parameterization in numerical models. This limits our ability to draw conclusions regarding aerosol-precipitation effects and essentially precludes the extrapolation of our findings to larger-scale scenarios. In addition, the fraction of global precipitation systems that could reasonably be compared with that of the Amazon region is unknown. Despite the limitations of the present study and of atmospheric models in general, such models are absolutely necessary as tools for improving our understanding of the impact of human activities, as well as for interpreting and validating the empirical relationships identified through observational analysis. Higher resolution might allow better representation of atmospheric processes and thereby provide more conclusive results, despite the complex manner in which the precipitation process responds to the atmosphere. Data obtained through modeling studies, including the present study, have indicated the potential significance of the role that aerosols play in the climate system. Clouds react to atmospheric properties in a complex way, aerosols being just one of the potential agents of change. As pointed by *Khain et al.* [2008], many discrepancies between the results reported in different observational and numerical studies can be attributed to the different atmospheric conditions and cloud types analyzed.

[63] **Acknowledgments.** This study received financial support in the form of a grants from the Conselho Nacional de Desenvolvimento Científico e Tecnológico (CNPq, National Council for Scientific and Technological Development; grant. 141479/2002-7), the Financiadora de Estudos e Projetos (FINEP, Funding Body for Studies and Projects) and the Fundaço de Amparo a Pesquisa do Estado de São Paulo (FAPESP, Foundation for the Support of Research in the state of São Paulo).

References

Ackerman, A. S., O. B. Toon, J. P. Taylor, D. W. Johnson, P. V. Hobbs, and R. J. Ferek (2000), Effects of aerosols on cloud albedo: Evaluation of Twomey's parameterization of cloud susceptibility using measurements of ship tracks, *J. Atmos. Sci.*, *57*, 2684–2695, doi:10.1175/1520-0469(2000)057<2684:EOAOCA>2.0.CO;2.

Ackerman, A. S., O. B. Toon, D. E. Stevens, and J. A. Coakley Jr. (2003), Enhancement of cloud cover and suppression of nocturnal drizzle in stratocumulus polluted by haze, *Geophys. Res. Lett.*, *30*(7), 1381, doi:10.1029/2002GL016634.

Albrecht, B. (1989), Aerosols, cloud microphysics, and fractional cloudiness, *Science*, *245*, 1227–1230, doi:10.1126/science.245.4923.1227.

Altaratz, O., I. Koren, T. Reisin, A. Kostinski, G. Feingold, Z. Levin, and Y. Yin (2008), Aerosols' influence on the interplay between condensation, evaporation and rain in warm cumulus cloud, *Atmos. Chem. Phys.*, *8*, 15–24.

Anderson, T. L., R. J. Charlson, S. E. Schwartz, R. Knutti, O. Boucher, H. Rodhe, and J. Heintzenberg (2003), Climate forcing by aerosols—A hazy picture, *Science*, *300*, 1103–1104, doi:10.1126/science.1084777.

Andreae, M. O., D. Rosenfeld, P. Artaxo, A. A. Costa, G. P. Frank, K. M. Longo, and M. A. F. Silva-Dias (2004), Smoking rain clouds over the Amazon, *Science*, *303*, 1337–1342, doi:10.1126/science.1092779.

Berry, E. X., and R. L. Reinhardt (1974a), Analysis of cloud drop growth by collection. Part I: Double distributions, *J. Atmos. Sci.*, *31*, 1814–1824, doi:10.1175/1520-0469(1974)031<1814:AAOCDG>2.0.CO;2.

Berry, E. X., and R. L. Reinhardt (1974b), Analysis of cloud drop growth by collection. Part II: Single initial distributions, *J. Atmos. Sci.*, *31*, 1825–1831, doi:10.1175/1520-0469(1974)031<1825:AAOCDG>2.0.CO;2.

Boucher, O., and U. Lohmann (1995), The sulfate-CCN-cloud albedo effect: A sensitivity study with two general circulation models, *Tellus, Ser.B*, *47*, 281–300.

Breon, F.-M., and M. Doutriaux-Boucher (2005), A comparison of cloud droplet radii measured from space, *IEEE Trans. Geosci. Remote Sens.*, *43*, 1796–1805, doi:10.1109/TGRS.2005.852838.

Chen, C., and W. R. Cotton (1983), A one-dimensional simulation of the strato-cumulus-capped mixed layer, *Boundary Layer Meteorol.*, *25*, 289–321, doi:10.1007/BF00119541.

Cotton, W. R., G. Tripoli, R. M. Rauber, and E. A. Mulvihill (1986), Numerical simulation of the effects of varying ice crystal nucleation rates and aggregation processes on orographic snowfall, *J. Clim. Appl. Meteorol.*, *25*, 1658–1680, doi:10.1175/1520-0450(1986)025<1658:NSOTEO>2.0.CO;2.

Cotton, W. R., et al. (2003), RAMS 2001: Current status and future directions, *Meteorol. Atmos. Phys.*, *82*, 5–29, doi:10.1007/s00703-001-0584-9.

DeMott, P. J., M. P. Meyers, and W. R. Cotton (1994), Parameterization and impact of ice initiation processes relevant to numerical model simulations of cirrus clouds, *J. Atmos. Sci.*, *51*, 77–90, doi:10.1175/1520-0469(1994)051<0077:PAIOII>2.0.CO;2.

Dolman, A. J., M. A. Silva Dias, J.-C. Calvet, M. Ashby, A. S. Tahara, C. Delire, P. Kabat, G. A. Fisch, and C. A. Nobre (1999), Meso-scale effects of tropical deforestation in Amazonia: Preparatory LBA modelling studies, *Ann. Geophys.*, *17*, 1095–1110, doi:10.1007/s00585-999-1095-0.

Flatau, P. J., G. J. Tripoli, J. Verlinde, and W. R. Cotton (1989), The CSU-RAM cloud microphysics model module: General theory and code documentation, *Tech. Rep. 451*, Dep. of Atmos. Sci., Colo. State Univ., Fort Collins.

Freitas, E. D., L. D. Martins, P. L. Silva Dias, and M. F. Andrade (2005), A simple photochemical module implemented in rams for tropospheric ozone concentration forecast in the metropolitan area of São Paulo, Brazil: Coupling and validation, *Atmos. Environ.*, *39*, 6352–6361, doi:10.1016/j.atmosenv.2005.07.017.

Freitas, S. R., K. M. Longo, R. Chatfield, D. Lathan, M. A. F. Silva Dias, M. O. Andreae, E. Prins, J. C. Santos, R. Gielow, and J. A. Carvalho Jr. (2006), Including the sub-grid scale plume rise of vegetation fires in low-resolution atmospheric transport models, *Atmos. Chem. Phys. Discuss.*, *8*, 11,521–11,559.

Freitas, S. R., et al. (2007), The coupled aerosol and tracer transport model to the Brazilian developments on the Regional Atmospheric Modeling System (CATT-BRAMS). Part 1: Model description and evaluation, *Atmos. Chem. Phys. Discuss.*, *7*, 8525–8569.

Gevaerd, R., S. R. Freitas, K. M. Longo, D. S. Moreira, M. A. F. Silva Dias, and P. L. Silva Dias (2006), Estimativa operacional da umidade de solo para iniciação de modelos de previsão numérica da atmosfera - Parte I: Impacto da umidade de solo e da parametrização de cumulus na simulaço de uma linha seca, *Rev. Bras. Meteorol.*, *21*, 74–88.

Gonçalves, F. L. T., J. A. Martins, and M. A. F. Silva Dias (2008), Shape parameter analysis using cloud spectra and gamma functions in the numerical modeling RAMS during LBA Project at Amazonian region, Brazil, *Atmos. Res.*, *89*, 1–11, doi:10.1016/j.atmosres.2007.12.005.

Grell, G. A. (1993), Prognostic evaluation of assumptions used by cumulus parameterizations, *Mon. Weather Rev.*, *121*, 764–787, doi:10.1175/1520-0493(1993)121<0764:PEOAUB>2.0.CO;2.

Hallett, J., and S. C. Mossop (1974), Production of secondary ice particles during the riming process, *Nature*, *249*, 26–28, doi:10.1038/249026a0.

Hansen, J. E., M. Sato, and R. Ruedy (1997), Radiative forcing and climate response, *J. Geophys. Res.*, *102*, 6831–6864, doi:10.1029/96JD03436.

Jacobson, M. Z. (2002), Control of fossil-fuel particulate black carbon and organic matter: Possibly the most effective method of slowing global warming, *J. Geophys. Res.*, *107*(D19), 4410, doi:10.1029/2001JD001376.

Jiang, H., and G. Feingold (2006), The effect of aerosol on warm convective clouds: Aerosol-cloud-surface flux feedbacks in a new coupled large eddy model, *J. Geophys. Res.*, *111*, D01202, doi:10.1029/2005JD006138.

Jiang, H., H. Xue, A. Teller, G. Feingold, and Z. Levin (2006), Aerosol effects on the lifetime of shallow cumulus, *Geophys. Res. Lett.*, *33*, L14806, doi:10.1029/2006GL026024.

Kaufman, Y. J., and R. S. Fraser (1997), The effect of smoke particles on clouds and climate forcing, *Science*, *277*, 1636–1639, doi:10.1126/science.277.5332.1636.

Kaufman, Y. J., and T. Nakajima (1993), Effect of Amazon smoke on cloud microphysics and albedo—Analysis from satellite imagery, *J. Appl. Meteorol.*, *32*, 729–744, doi:10.1175/1520-0450(1993)032<0729:EOASOC>2.0.CO;2.

Kawamoto, K. (2006), Relationships between cloud properties and precipitation amount over the Amazon basin, *Atmos. Res.*, *82*, 239–247, doi:10.1016/j.atmosres.2005.10.007.

Kawamoto, K., and T. Nakajima (2003), Seasonal variation of cloud particle size as derived from AVHRR remote sensing, *Geophys. Res. Lett.*, *30*(15), 1810, doi:10.1029/2003GL017437.

Khain, A. P., and A. Pokrovsky (2004), Simulation of effects of atmospheric aerosols on deep turbulent convective clouds using a spectral microphysics mixed-phase cumulus cloud model. Part II: Sensitivity studies, *J. Atmos. Sci.*, *61*, 2983–3001, doi:10.1175/JAS-3281.1.

Khain, A. P., M. Ovtchinnikov, M. Pinsky, A. Pokrovsky, and H. Krugliak (2000), Notes on the state-of-the-art numerical modeling of cloud microphysics, *Atmos. Res.*, *55*, 159–224.

Khain, A. P., D. Rosenfeld, and A. Pokrovsky (2003), Simulations of aerosol effects on convective clouds developed under continental and maritime conditions, paper presented at EUG Joint Assembly, Nice, France.

Khain, A. P., D. Rosenfeld, and A. Pokrovsky (2005), Aerosol impact on the dynamics and microphysics of convective clouds, *Q. J. R. Meteorol. Soc.*, *131*, 2639–2663, doi:10.1256/qj.04.62.

Khain, A. P., N. BenMoshe, and A. Pokrovsky (2008), Factors determining the impact of aerosols on surface precipitation from clouds: An attempt at classification, *J. Atmos. Sci.*, *65*, 1721–1748, doi:10.1175/2007JAS2515.1.

Klemp, J. B., and R. B. Wilhelmson (1978), The simulation of three-dimensional convective storm dynamics, *J. Atmos. Sci.*, *35*, 1070–1096, doi:10.1175/1520-0469(1978)035<1070:TSOTDC>2.0.CO;2.

Koren, I., Y. J. Kaufman, L. A. Remer, and J. V. Martins (2004), Measurements of the effect of Amazon smoke on inhibition of cloud formation, *Science*, *303*, 1342–1345, doi:10.1126/science.1089424.

Lee, S. S., L. J. Donner, V. T. Phillips, and Y. Ming (2008), Examination of aerosol effects on precipitation in deep convective clouds during the 1997 ARM summer experiment, *Q. J. R. Meteorol. Soc.*, *134*, 1201–1220.

Liljegren, J. C., and B. M. Lesht (1996), Measurements of integrated water vapor and cloud liquid water from microwave radiometers at the DOE ARM cloud and radiation testbed in the Southern Great Plains, paper presented at International Geoscience Remote Sensing Symposium, Inst. for Electr. and Electron. Eng., Lincoln, Nebr.

Lin, J. C., T. Matsui, R. A. Pielke Sr., and C. Kummerow (2006), Effects of biomass burning-derived aerosols on precipitation and clouds in the Amazon Basin: A satellite-based empirical study, *J. Geophys. Res.*, *111*, D19204, doi:10.1029/2005JD006884.

Lohmann, U., and J. Feichter (2005), Global indirect aerosol effects: A review, *Atmos. Chem. Phys.*, *5*, 715–737.

Lohmann, U., J. Quaas, S. Kinne, and J. Feichter (2007), Different approaches for constraining global climate models of the anthropogenic indirect aerosol effect, *Bull. Am. Meteorol. Soc.*, *88*, 243–249, doi:10.1175/BAMS-88-2-243.

Lynn, B. H., A. P. Khain, J. Dudhia, D. Rosenfeld, A. Pokrovsky, and A. Seifert (2005a), Spectral (bin) microphysics coupled with a mesoscale model (MM5). Part I: Model description and first results, *Mon. Weather Rev.*, *133*, 44–58, doi:10.1175/MWR-2840.1.

Lynn, B. H., A. P. Khain, J. Dudhia, D. Rosenfeld, A. Pokrovsky, and A. Seifert (2005b), Spectral (bin) microphysics coupled with a mesoscale model (MM5). Part II: Simulation of a cape rain event with a squall line, *Mon. Weather Rev.*, *133*, 59–71, doi:10.1175/MWR-2841.1.

Marchand, R., T. Ackerman, E. R. Westwater, S. A. Clough, K. Cady-Pereira, and J. C. Liljegren (2003), An assessment of microwave absorption models and retrievals of cloud liquid water using clear-sky data, *J. Geophys. Res.*, *108*(D24), 4773, doi:10.1029/2003JD003843.

Martins, J. A., F. L. T. Gonçalves, and M. A. F. Silva Dias (2004), Cloud condensation nuclei in clear and polluted atmospheric conditions in the Amazonian region, paper presented at 14th International Conference on Clouds and Precipitation, Int. Assoc. of Meteorol. and Atmos. Sci., Bologna, Italy.

Mellor, G. L., and T. Yamada (1974), A hierarchy of turbulence closure models for planetary boundary layers, *J. Atmos. Sci.*, *31*, 1791–1806, doi:10.1175/1520-0469(1974)031<1791:AHOTCM>2.0.CO;2.

Mellor, G. L., and T. Yamada (1982), Development of a turbulence closure model for geophysical fluid problems, *Rev. Geophys.*, *20*, 851–875, doi:10.1029/RG020i004p00851.

Meneguzzo, F., M. Pasqui, G. Menduni, G. Messeri, B. Gozzini, D. Grifoni, M. Rossi, and G. Maracchi (2004), Sensitivity of meteorological high-resolution numerical simulations of the biggest floods occurred over the Arno river basin, Italy, in the 20th century, *J. Hydrol.*, *288*, 37–56, doi:10.1016/j.jhydrol.2003.11.032.

Meyers, M. P., P. J. DeMott, and W. R. Cotton (1992), New primary ice nucleation parameterizations in an explicit cloud model, *J. Appl. Meteorol.*, *31*, 708–721, doi:10.1175/1520-0450(1992)031<0708:NPINPI>2.0.CO;2.

Meyers, M. P., R. L. Walko, J. Y. Harrington, and W. R. Cotton (1997), New RAMS cloud microphysics parameterization. Part II: The two-moment scheme, *Atmos. Res.*, *45*, 3–39, doi:10.1016/S0169-8095(97)00018-5.

Mossop, S. C. (1976), Production of secondary ice particles during the growth of graupel by riming, *Q. J. R. Meteorol. Soc.*, *102*, 45–57, doi:10.1002/qj.49710243104.

Nober, F. J., H.-F. Graf, and D. Rosenfeld (2003), Sensitivity of the global circulation to the suppression of precipitation by anthropogenic aerosols, *Global Planet. Change*, *37*, 57–80, doi:10.1016/S0921-8181(02)00191-1.

Penner, J. E., J. Quaas, T. Storelvmo, T. Takemura, O. Boucher, H. Guo, A. Kirkevag, J. E. Kristjánsson, and O. Seland (2006), Model intercomparison of indirect aerosol effects, *Atmos. Chem. Phys.*, *6*, 3391–3405.

Phillips, V., A. Khain, and A. Pokrovsky (2007), The influence of melting on the dynamics and precipitation production in maritime and continental storm-clouds, *J. Atmos. Sci.*, *64*, 338–359, doi:10.1175/JAS3832.1.

Pielke, R. E., et al. (1992), A comprehensive meteorological modeling system–RAMS, *Meteorol. Atmos. Phys.*, *49*, 69–91, doi:10.1007/BF01025401.

Platnick, S., M. D. King, S. A. Ackerman, W. P. Menzel, B. A. Baum, and R. A. Frey (2003), The MODIS cloud products: Algorithms and examples from Terra, *IEEE Trans. Geosci. Remote Sens.*, *41*, 459–473, doi:10.1109/TGRS.2002.808301.

Procopio, A. S., P. Artaxo, Y. J. Kaufman, L. A. Remer, J. S. Schafer, and B. N. Holben (2004), Multiyear analysis of amazonian biomass burning smoke radiative forcing of climate, *Geophys. Res. Lett.*, *31*, L03108, doi:10.1029/2003GL018646.

Ramanathan, V., and G. Carmichael (2008), Global and regional climate changes due to black carbon, *Nat. Geosci.*, *1*, 221–227, doi:10.1038/ngeo156.

Reisin, T., S. Tzivion, and Z. Levin (1996), Seeding convective clouds with ice nuclei or hygroscopic particles: A numerical study using a model with detailed microphysics, *J. Appl. Meteorol.*, *35*, 1416–1434, doi:10.1175/1520-0450(1996)035<1416:SCCWIN>2.0.CO;2.

Roberts, G. C., M. O. Andreae, J. Zhou, and P. Artaxo (2001), Cloud condensation nuclei in the Amazon Basin: "Marine" conditions over a continent?, *Geophys. Res. Lett.*, *28*(14), 2807–2810, doi:10.1029/2000GL012585.

Rosenfeld, D. (1999), TRMM observed first direct evidence of smoke from forest fires inhibiting rainfall, *Geophys. Res. Lett.*, *26*(20), 3105–3108, doi:10.1029/1999GL006066.

Rosenfeld, D. (2000), Suppression of rain and snow by urban and industrial pollution, *Science*, *287*, 1793–1796, doi:10.1126/science.287.5459.1793.

Rosenfeld, D., and I. M. Lensky (1998), Satellite-based insights into precipitation formation processes in continental and maritime convective clouds, *Bull. Am. Meteorol. Soc.*, *79*, 2457–2476, doi:10.1175/1520-0477(1998)079<2457:SBIIPF>2.0.CO;2.

Rosenfeld, D., Y. J. Kaufman, and I. Koren (2006), Switching cloud cover and dynamical regimes from open to closed Benard cells in response to the suppression of precipitation by aerosols, *Atmos. Chem. Phys.*, *6*, 2503–2511.

Schuster, G. L., O. Dubovik, B. N. Holben, and E. E. Clothiaux (2005), Inferring black carbon content and specific absorption from Aerosol Robotic Network (AERONET) aerosol retrievals, *J. Geophys. Res.*, *110*, D10S17, doi:10.1029/2004JD004548.

Silva Dias, M. A. F., et al. (2002a), Clouds and rain processes in a biosphere atmosphere interaction context, *J. Geophys. Res.*, *107*(D20), 8072, doi:10.1029/2001JD000335.

Silva Dias, M. A. F., et al. (2002b), A case study of convective organization into precipitating lines in the Southwest Amazon during the WETAMC and TRMM-LBA, *J. Geophys. Res.*, *107*(D20), 8078, doi:10.1029/2001JD000375.

Stier, P., J. H. Seinfeld, S. Kinne, and O. Boucher (2007), Aerosol absorption and radiative forcing, *Atmos. Chem. Phys.*, *7*, 5237–5261.

Suzuki, K., T. Nakajima, A. Numaguti, T. Takemura, K. Kawamoto, and A. Higurashi (2004), A study of the aerosol effect on a cloud field with simultaneous use of GCM modeling and satellite observations, *J. Atmos. Sci.*, *61*, 179–194, doi:10.1175/1520-0469(2004)061<0179:ASOTAE>2.0.CO;2.

Tao, W.-K., X. Li, A. Khain, T. Matsui, S. Lang, and J. Simpson (2007), Role of atmospheric aerosol concentration on deep convective precipitation: Cloud-resolving model simulations, *J. Geophys. Res.*, *112*, D24S18, doi:10.1029/2007JD008728.

Teller, A., and Z. Levin (2006), The effects of aerosols on precipitation and dimensions of subtropical clouds: A sensitivity study using a numerical cloud model, *Atmos. Chem. Phys.*, *6*, 67–80.

Toon, O. B. (2000), How pollution suppresses rain, *Science*, *287*, 1763–1764, doi:10.1126/science.287.5459.1763.

Tripoli, G. J., and W. R. Cotton (1982), The Colorado State Univ. three-dimensional cloud mesoscale model, 1982: Part I: General theoretical framework and sensitivity experiments, *J. Rech. Atmos.*, *16*, 185–220.

Twomey, S. (1974), Pollution and the planetary albedo, *Atmos. Environ.*, *8*, 1251–1256, doi:10.1016/0004-6981(74)90004-3.

Twomey, S., and T. A. Wojciechowski (1969), Observations of geographical variation of cloud nuclei, *J. Atmos. Sci.*, *26*, 648–651, doi:10.1175/1520-0469(1969)26<648:OOTGVO>2.0.CO;2.

van den Heever, S. C., and W. R. Cotton (2007), Urban aerosol impacts on downwind convective storms, *J. Appl. Meteorol. Climatol.*, *46*, 828–850, doi:10.1175/JAM2492.1.

van den Heever, S. C., G. G. Carrió, W. R. Cotton, P. J. DeMott, and A. J. Prenni (2006), Impacts of nucleating aerosol on Florida storms. Part I: Mesoscale simulations, *J. Atmos. Sci.*, *63*, 1752–1775, doi:10.1175/JAS3713.1.

Verlinde, J., and W. R. Cotton (1993), Fitting microphysical observations of non-steady convective clouds to a numerical model: An application of the adjoint technique of data assimilation to a kinematic model, *Mon. Weather Rev.*, *121*, 2776–2793, doi:10.1175/1520-0493(1993)121<2776:FMOONC>2.0.CO;2.

Verlinde, J., P. J. Flatau, and W. R. Cotton (1990), Analytical solutions to the collection growth equation: Comparison with approximate methods and application to cloud microphysical parameterization schemes, *J. Atmos. Sci.*, *47*, 2871–2880, doi:10.1175/1520-0469(1990)047<2871:ASTTCG>2.0.CO;2.

Vestin, A., J. Rissler, E. Swietlicki, G. P. Frank, and M. O. Andreae (2007), Cloud-nucleating properties of the Amazonian biomass burning aerosol: Cloud condensation nuclei measurements and modeling, *J. Geophys. Res.*, *112*, D14201, doi:10.1029/2006JD008104.

Walko, R., W. R. Cotton, M. P. Meyers, and J. Y. Harrington (1995), New RAMS cloud microphysics parameterization. Part I: The single-moment scheme, *Atmos. Res.*, *38*, 29–62, doi:10.1016/0169-8095(94)00087-T.

Walko, R. L., et al. (2000), Coupled atmosphere-biophysics-hydrology models for environmental modeling, *J. Appl. Meteorol.*, *39*, 931–944, doi:10.1175/1520-0450(2000)039<0931:CABHMF>2.0.CO;2.

Wang, C. (2005), A modeling study of the response of tropical deep convection to the increase of cloud condensation nuclei concentration: 1. Dynamics and microphysics, *J. Geophys. Res.*, *110*, D21211, doi:10.1029/2004JD005720.

Williams, E., et al. (2002), Contrasting convective regimes over the Amazon: Implications for cloud electrification, *J. Geophys. Res.*, *107*(D20), 8082, doi:10.1029/2001JD000380.

Xue, H., and G. Feingold (2006), Large-eddy simulations of trade wind cumuli: Investigation of aerosol indirect effects, *J. Atmos. Sci.*, *63*, 1605–1622, doi:10.1175/JAS3706.1.

F. L. T. Gonçalves, Department of Atmospheric Science, University of São Paulo, São Paulo, SP, Brazil. (fgoncalv@model.iag.usp.br)

J. A. Martins, Department of Environmental Engineering, Federal University of Technology-Paraná, Rua Alagoas, 2001, Londrina, PR 86020-430, Brazil. (jmartins@utfpr.edu.br)

M. A. F. Silva Dias, Centro de Previsão de Tempo e Estudos Climáticos, Rodovia Presidente Dutra, km 40, Cachoeira Paulista, SP 12630-000, Brazil. (assuncao.dias@cptec.inpe.br)